Applied Mathematical Modelling 117 (2023) 316–335

Contents lists available at ScienceDirect

Applied Mathematical Modelling

journal homepage: www.elsevier.com/locate/apm

Non-reciprocal wave propagation in time-modulated elastic lattices with inerters

Danilo Karličić[a,*], Milan Cajić[a,b], Stepa Paunović[a], Aleksandar Obradović[c], Sondipon Adhikari[d], Johan Christensen[e]

[a] Mathematical Institute of the Serbian Academy of Sciences and Arts, 11000 Belgrade, Serbia
[b] Faculty of Science and Engineering, Swansea University, Swansea SA1 8EN, UK
[c] Faculty of Mechanical Engineering, University of Belgrade, 11000 Belgrade, Serbia
[d] James Watt School of Engineering, The University of Glasgow, Glasgow G12 8QQ, UK
[e] IMDEA Materials Institute, Calle Eric Kandel, 2, 28906, Getafe, Madrid, Spain

ARTICLE INFO

Article history:
Received 20 June 2022
Revised 13 December 2022
Accepted 16 December 2022
Available online 20 December 2022

Keywords:
Non-reciprocial wave propagation
Mechancial metamaterials
Phononic lattices
Inerters
Time-modulated properties
Coupled beams system

ABSTRACT

Non-reciprocal wave propagation in acoustic and elastic media has received much attention of researchers in recent years. This phenomenon can be achieved by breaking the reciprocity through space- and/or time-dependent constitutive material properties, which is an important step in overcoming the limitations of conventional acoustic- and phononic-like mechanical lattices. A special class of mechanical metamaterials with non-reciprocal wave transmission are latices with time-modulated mass and stiffness properties. Here, we investigate the non-reciprocity in elastic locally resonant and phononic-like one-dimensional lattices with inerter elements where mass and stiffness properties are simultaneously modulated through inerters and springs as harmonic functions of time. By considering the Bloch theorem and Fourier expansions, the frequency-band structures are determined for each configuration while asymmetric band gaps are found by using the weighting and threshold method. The reduction in frequency due to introduced inerters was observed in both phononic and locally resonant metamaterials. Dynamic analysis of finite-length lattices by the finite difference method revealed a uni-directional wave propagation. Special attention is given to phononic-like lattice based on a discrete-continuous system of multiple coupled beams. Moreover, the existence of edge modes in the discrete phononic lattice is confirmed through the bulk-edge correspondence and their time evolution quantified by the topologically invariant Chern number. The proposed methodology used to investigate non-reciprocal wave transmission in one-dimensional inerter-based lattices can be extended to study more complex two-dimensional lattices.

1. Introduction

Recent progress in metamaterials and phononic systems with unique mechanical properties provides great opportunities for new designs in different fields such as civil, mechanical and aerospace engineering and bio-engineering [1]. These applications are often based on the control of acoustic and elastic wave propagation properties or vibration attenuation capabili-

* Corresponding author.
E-mail address: danilok@mi.sanu.ac.rs (D. Karličić).

https://doi.org/10.1016/j.apm.2022.12.029
0307-904X/

ties both in lower and higher frequency ranges. Some cutting-edge examples include novel meta- implants and biomaterials [2], sensing devices, mechanical diodes and energy harvesters [3]. Similarly as with their firstly discovered counterparts in solid-state physics and electromagnetism, the mechanical metamaterials' unique wave propagation properties come from their internal architecture and spatial periodicity. The main difference between phononic crystals (PC) and acoustic metamaterials (AMM) in their classical setup is that the latter can have locally resonant substructures, which enables one to create and manipulate band gaps at lower frequency regimes [4]. This is important for the control of wave propagation properties in vibration isolation, seismic wave attenuation and energy harvesting applications [5]. Most of the unique wave propagation properties of the aforementioned media appear due to the special periodicity and material properties of their representative unit cells (UC). This means that one can manipulate their special properties to achieve some intriguing phenomena such as the topological pumping of edge modes [6] through spatial modulation of stiffness, or the Hofstadter butterfly effect [7] by introducing quasi-periodicity.

The uni-directional wave propagation property of a special class of metamaterials with space-time modulated material characteristics is based on the broken reciprocity [8]. Namely, reciprocity in elastodynamics and acoustics usually denotes the property of a medium that the frequency response measured between two points does not change when the source and the receiver switch places. This property is also considered to be robust in terms of energy losses and inhomogeneities in the material. However, by modulating the periodic media properties one can break the reciprocity and achieve unique dynamical characteristics, which are manifested in asymmetric band gaps and uni-directional transfer of wave energy for a given excitation frequency. There are numerous applications of non-reciprocal wave propagation in the design of new devices in electromagnetics such as circulators, frequency mixer, one-way beam splitters, non-reciprocal antennas [9], and many other analogous examples in mechanics [10], electro-mechanics [11], magneto-elastic systems [12] and acoustics [13]. From the theoretical point of view, the band structure properties of such systems can be investigated by considering different mathematical approaches. The most common approach is based on the Floquet-Bloch theorem [14] in conjunction with the Fourier expansion, which was applied to study discrete mechanical lattices with time-modulated stiffness [15] and mass properties [16], or both of these properties modulated simultaneously [17]. In [18], another approach based on the asymptotic approximation and perturbation method was applied for dispersion analysis, one-way wave transmission, amplification and wave-blocking. For continuous structures, the plane wave expansion method (PWEM) found great application in the determination of the asymmetrical band-gaps in space-time modulated structural elements such as rod, beam, membranes, and plates [10,19–21]. The PWEM is shown to be very useful in understanding the wave propagation through the axially moving rod with space-time varying properties [22].

The concept of time-modulated materials has inspired many researchers to use these properties for control of wave energy and uni-directional propagation [23,24]. The most common approach in time modulation of material properties is based on imposed external fields, where a high modulation speed comparable to the wave propagation velocity can be achieved. Another way includes piezoelectric patches, where the stiffness of the beam can be modulated in time through the negative capacitance shunts and controlled by a switching circuit [25]. In [26], metamaterial beam properties are modulated based on the array of periodically distributed magnets and coils, where magnets are rigidly bonded to the host beam whereas coils are elastically attached to it through a pair of flexible cantilevers. The electro-actuated metamaterial beam with attached resonators was introduced in [27]. However, metamaterials with time-modulated mass properties are much more difficult to produce in practice. In [16,17], the time-modulation of stiffness and mass properties of the PC type of lattice was proposed based on moving point masses within the UCs and without any externally applied field. Moreover, the authors used the Bloch-Fourier procedure to determine the dispersion characteristics and study the uni-directional wave propagation. Another study [28] shows uni-directional wave propagation in AMM lattices with time-modulated mass and stiffness properties. Interesting models of mechanical and electro-mechanical systems with time-modulated mass or stiffness properties were proposed in the first chapter of the book [29]. In the present work, time-dependent mass properties will be introduced through time-modulated ideal inerters that can be used in both phononic and locally resonant metamaterial lattices [30,31].

The first appearance of inerters as structural elements is related to the work of Smith [32,33], that was later experimentally verified in [34]. Two comprehensive review studies [35,36] showed a number of interesting applications and practical realizations of different types of inerters ranging from purely mechanical, to combinations of mechanical and hydraulic, as well as electro-mechanical inerters. Their application in engineering includes mostly, but is not limited to, vibration attenuation. The introduction of the inerter into the structural model as the vibration absorber is very often related to the demands for improved performance and reduced weight and size of the system, which makes them almost ideal candidates to be incorporated into metamaterials. Inerter-based discrete lattice model in the form of AMM was introduced in [37] to study its effect on longitudinal wave propagation. The authors have demonstrated how the inerter can contribute to both the up-shift and down-shift of the band gap frequency range. Further, the inerter-based lattices and locally resonant structures showed a great application in a special class of seismic metamaterials for low-frequency wave propagation control as shown in [30,38]. In [39] it was demonstrated how inerters introduced in local resonators attached to the elastic beam structure can broaden the low-frequency band gaps. Moreover, in [31] the authors showed how the band gap widths and responses of AMMs and PCs are directly dependent on the location and magnitude of the inerter elements.

In this work, we systematically investigate the uni-directional wave propagation in inerter-based lattices with time-modulated mass, inertance, and stiffness properties. Time modulation of mass properties is performed through the inerter elements introduced into discrete models of mass-spring systems in their phononic and locally resonant lattice setup. Moreover, a uni-directional waveguide based on the system of multiple beams coupled through discrete spring and inerter ele-

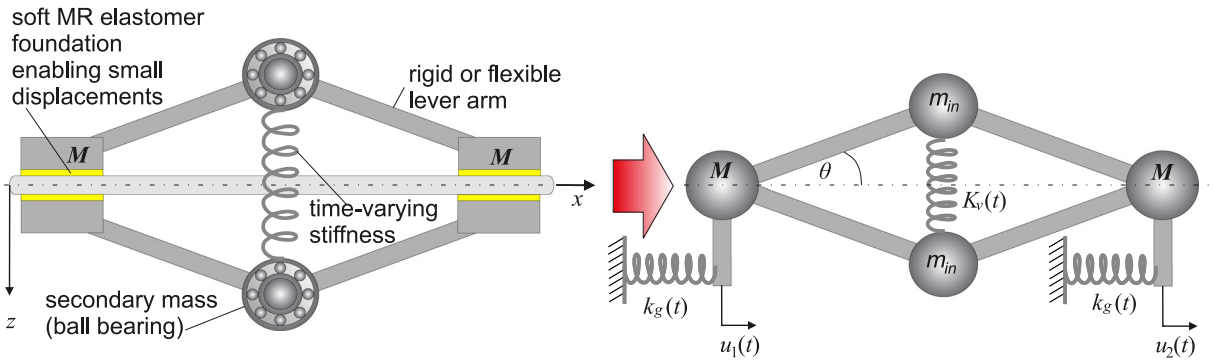

Fig. 1. Illustration of the possible physical model of a mechanical inerter device..

ments with time-modulated stiffness and inertance properties is investigated for the first time. By considering the Floquet-Bloch theorem and the Fourier expansion, the initial system of motion equations is reduced to the quadratic eigenvalue problem. The obtained band structures are used to investigate asymmetric band gaps. The finite difference method is employed to obtain time responses and demonstrate the uni-directional wave propagation. Moreover, we revealed the existence of topologically protected one-way edge modes by using the principle of bulk-edge correspondence. Finally, the topologically invariant Chern number is calculated for discrete phononic lattices to quantify the time evolution of edge modes in the configuration with inerter elements.

2. The inerter-based lattices with time-modulated inertance and stiffness properties

2.1. Introduction to inerters and time-modulation of mechanical properties

In the literature, the authors have proposed many different designs of mechanical inerter devices. Some of them include ball-screw-based inerters [33] while another more simple design is based on levered secondary masses [40] connected through rigid links to that of an independent degree of freedom in the direction normal to the transverse axis. One such inerter is illustrated in Fig. 1, where secondary masses are denoted as m_{in} while the angle between the rigid links and the base is θ. The main issue is how to achieve time-modulated properties of such inerter devices. One approach can include the introduction of a linear time-varying spring of stiffness $K_v(t)$, which is connecting two secondary masses (see Fig. 1 left). One can also apply a combination of permanent and electromagnets that can be represented by a nonlinear equivalent spring (e.g. see [41]). According to Banerjee et al. [40], Hussein et al. [42], if such inerters are implemented into the one-dimensional lattice and under the assumption of small displacements, the force acting from inertial amplifier onto the baseline mass along the direction of the wave propagation could be defined as

$$F_{in}(t) = \frac{m_{in}(\ddot{u}_2 - \ddot{u}_1) + 2K_v(t)(u_2 - u_1)}{4\tan^2(\theta)}, \tag{1}$$

where $u_{1,2}$ are displacements of the baseline masses. Here, one can notice that this force depends on the values of secondary masses, the stiffness of the spring connecting these masses, and the angle between the lever arm and the baseline. If the value of the spring $K_v(t)$ is varied with time, the force will also vary with it. This stiffness will mainly contribute to the stiffness matrix and therefore we can speak only about the time-modulated stiffness properties. In a similar manner, one can achieve time-modulated ground springs by using the soft magnetorheological (MR) elastomer foundation between the mass and the fixed baseline that produces the force proportional to the stiffness $k_g(t)$ of the spring and varied with the exerted magnetic field. However, to directly achieve time-modulation of the inertance one should be able to vary mass with time which is very difficult to achieve in practice, and somehow different designs of inerter devices need to be suggested (see [29], p. 10). Therefore, for the sake of clarity, in this work, we are only dealing with non-dimensional time-varying parameters in order to investigate their effect on uni-directional wave propagation without going into details about their physicality.

For the purpose of further analysis, we will consider the phononic-like mass-spring-inerter lattice illustrated in (Fig. 2a) and similar inerter-based mass-in-mass locally resonant lattice given in (Fig. 2b). These lattices consist of periodically distributed unit cells of mass-spring-inerter sub-systems connected into an infinite dimensional chain. Therefore, the main difference between these two chain models is the presence of internal resonators in the case of unit cells with mass-in-mass sub-systems. In order study the Bloch wave propagation, the first step is to form an infinite dimensional chain and define the corresponding periodic boundary conditions. Figure 2 shows the corresponding nth unit cell (UC) of the phononic lattice (PL) and locally resonant lattice (LRL) confined by red dashed rectangles. For the presented PL model, the UC consists of three identical masses connected with different time-modulated springs and inerters. Moreover, each point mass is con-

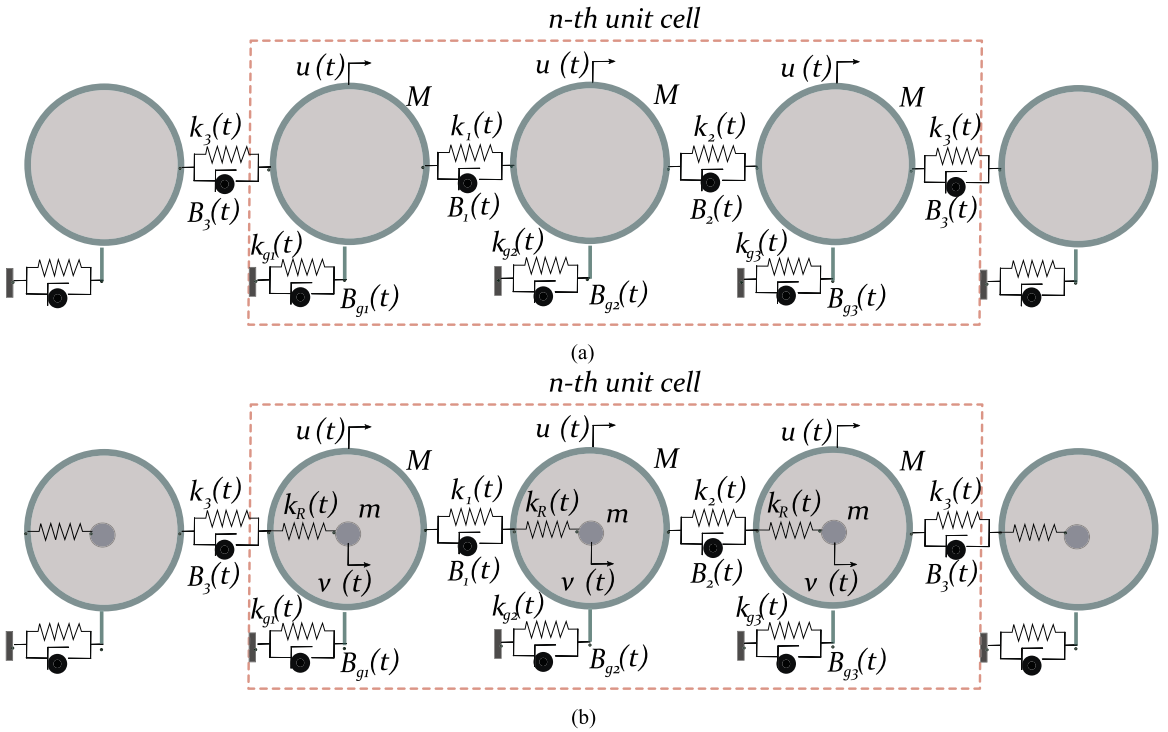

Fig. 2. The inerter-based one-dimensional lattices constituted of periodically placed mass-spring-inerter elements with time-modulated stiffness and inerter properties: (a) phononic lattice, and (b) locally resonant metamaterial chain. The unit cell (confined by a red dashed rectangle) consists of three masses (phononic case) or three mass-in-mass sub-systems (locally resonant case) interconnected with spring and inerter elements. (For interpretation of the references to colour in this figure legend, the reader is referred to the web version of this article.)

nected to a fixed base by a time-modulated spring and inerter. Furthermore, UC of the LRL has a similar design, except for the added internal resonators, each of them connected to the host mass by an additional time-modulated spring.

2.2. Problem formulation

The governing equations of the general case of the locally resonant lattice with time-varying stiffness and inerter properties for the nth UC (Fig. 2b) can be expressed in a general case as a system of ordinary differential equations with time-dependent coefficients as follows

$$M\ddot{u}_r^n + k_{r-1}(t)(u_r^n - u_{r-1}^n) + k_r(t)(u_r^n - u_{r+1}^n) + k_{gr}(t)u_r^n + k_{Rr}(t)(u_r^n - v_r^n) + \tag{2}$$

$$B_{r-1}(t)(\ddot{u}_r^n - \ddot{u}_{r-1}^n) + B_r(t)(\ddot{u}_r^n - \ddot{u}_{r+1}^n) + B_{gr}(t)\ddot{u}_r^n +$$

$$\dot{B}_{r-1}(t)(\dot{u}_r^n - \dot{u}_{r-1}^n) + \dot{B}_r(t)(\dot{u}_r^n - \dot{u}_{r+1}^n) + \dot{B}_{gr}(t)\dot{u}_r^n = 0,$$

$$m\ddot{v}_r^n + k_{Rr}(t)(v_r^n - u_r^n) = 0, \tag{3}$$

where $r = 1, \ldots, R$, R is the number of masses in the nth unit cell. In general, the following terms denoted by u_r^n, u_{r-1}^n and u_{r+1}^n are related to displacements of the masses of nth unit cell in the direction of wave propagation. The term v_r^n is related to displacements of the internal mass resonators. The values of all outer masses are equal and denoted by M while the values of internal masses are also equal and denoted by m. Time-modulated parameters are given as time-dependent functions in the case of stiffness as $k_r(t)$, inertance $B_r(t)$, ground stiffness $k_{gr}(t)$ and ground inertance as $B_{gr}(t)$. In order to study the non-reciprocal wave propagation through the time-varying one-dimensional lattice structures, we will limit our analysis only to the case when $R = 3$, i.e. the case with only three masses within the unit cell of PL or three mass-in-mass sub-systems in the case of LRL (see Fig. 2b). It should be mentioned that equations for the phononic lattice can be recovered by neglecting the equation Eq. (3) and corresponding displacements of internal resonators. Moreover, when the index of the displacement u_r^n, take the values $r = 0$ or $r > R$, then the index and exponent of the displacement will be changed according to the following, $u_0^n \to u_3^{n-1}$ and $u_4^n \to u_1^{n+1}$.

The time-dependent coefficients are adopted in the harmonic form as

$$k_r(t) = k_0(1+\beta_m\Gamma_r(t)) = k_0 C_r(t), \quad k_{gr}(t) = k_0\gamma_g(1+\beta_{gm}\Gamma_r(t)) = k_0\gamma_g D_r(t), \tag{4}$$

$$k_{Rr}(t) = k_0\xi_R(1+\theta_m\Gamma_r(t)) = k_0\xi_R G_r(t),$$

$$B_r(t) = sM(1+\rho_m\Gamma_r(t)) = sMV_r(t), \quad B_{gr}(t) = \epsilon_g M(1+\rho_{gm}\Gamma_r(t)) = \epsilon_g M W_r(t), \tag{5}$$

$$\dot{B}_r(t) = sM\rho_m\dot{\Gamma}_r(t) = sM\omega_m E_r(t), \quad \dot{B}_{gr}(t) = \epsilon_g M\rho_{gm}\dot{\Gamma}_r(t) = \epsilon_g M\omega_m F_r(t),$$

where $\Gamma_r(t) = \cos(\omega_m t + \phi_r)$, $\phi_r = \frac{2\pi r}{R}$, $r = 1, 2, \ldots R$ and ω_m is the frequency of modulation. In the above equations, the following material constants are given: k_0 is the stiffness coefficient, β_m is the stiffness ratio, γ_g and β_{gm} are ground spring stiffness ratios, θ_m and ξ_R, are stiffness ratios of internal resonators. The parameters related to time-modulated inerters are the inter-mass ratios s and ρ_m while corresponding ratios ϵ_g and ρ_{gm} are related to grounded inerters. The relation between the masses of outer and inner elements in the UC is given by $b = m/M$. By introducing the Eqs. (4) and (5) into the system of differential equations with time-dependent coefficients Eqs. (2) and (3), a new system of equations is obtained in the matrix form as

$$\frac{1}{\omega_0^2}\mathbf{M}(t)\ddot{\mathbf{u}}_n + \frac{\Omega_m}{\omega_0}\mathbf{C}(t)\dot{\mathbf{u}}_n + \mathbf{K}(t)\mathbf{u}_n + \tag{6}$$

$$\frac{1}{\omega_0^2}\mathbf{M}^{(l)}(t)\ddot{\mathbf{u}}_{n-1} + \frac{\Omega_m}{\omega_0}\mathbf{C}^{(l)}(t)\dot{\mathbf{u}}_{n-1} + \mathbf{K}^{(l)}(t)\mathbf{u}_{n-1} +$$

$$\frac{1}{\omega_0^2}\mathbf{M}^{(r)}(t)\ddot{\mathbf{u}}_{n+1} + \frac{\Omega_m}{\omega_0}\mathbf{C}^{(r)}(t)\dot{\mathbf{u}}_{n+1} + \mathbf{K}^{(r)}(t)\mathbf{u}_{n+1} = \mathbf{0}$$

where $\mathbf{M}(t)$ and $\mathbf{K}(t)$ are time-dependent mass and stiffness matrices of the unit cell, respectively, the matrix $\mathbf{C}(t)$ is related to the time-modulated inerter properties, $\mathbf{u}_n$ is the vector of displacements, natural frequency of a single oscillator is given as $\omega_0^2 = k_0/M$ while $\Omega_m = \omega_m/\omega_0$ represents the dimensionless modulated frequency. The interaction of the nth UC with other UCs in the lattice is given through the left and right interactions of the mass, stiffness, and time-modulated inerter matrices expressed as $\mathbf{M}^{(l)}(t)$, $\mathbf{K}^{(l)}(t)$, $\mathbf{C}^{(l)}(t)$ and $\mathbf{M}^{(r)}(t)$, $\mathbf{K}^{(r)}(t)$, $\mathbf{C}^{(r)}(t)$.

The time-dependent mass and stiffness matrices are obtained as

$$\mathbf{M}(t) = \begin{bmatrix} Q_1(t) & -sV_1(t) & 0 & 0 & 0 & 0 \\ -sV_1(t) & Q_2(t) & -sV_2(t) & 0 & 0 & 0 \\ 0 & -sV_2(t) & Q_3(t) & 0 & 0 & 0 \\ 0 & 0 & 0 & b & 0 & 0 \\ 0 & 0 & 0 & 0 & b & 0 \\ 0 & 0 & 0 & 0 & 0 & b \end{bmatrix}, \tag{7}$$

$$\mathbf{K}(t) = \begin{bmatrix} P_1(t) & -C_1(t) & 0 & -\xi_R G_1(t) & 0 & 0 \\ -C_1(t) & P_2(t) & -C_2(t) & 0 & -\xi_R G_2(t) & 0 \\ 0 & -C_2(t) & P_3(t) & 0 & 0 & -\xi_R G_3(t) \\ -\xi_R G_1(t) & 0 & 0 & \xi_R G_1(t) & 0 & 0 \\ 0 & -\xi_R G_2(t) & 0 & 0 & \xi_R G_2(t) & 0 \\ 0 & 0 & -\xi_R G_3(t) & 0 & 0 & \xi_R G_3(t) \end{bmatrix}, \tag{8}$$

$$\mathbf{C}(t) = \begin{bmatrix} Z_1(t) & -sE_1(t) & 0 & 0 & 0 & 0 \\ -sE_1(t) & Z_2(t) & -sE_2(t) & 0 & 0 & 0 \\ 0 & -sE_2(t) & Z_3(t) & 0 & 0 & 0 \\ 0 & 0 & 0 & 0 & 0 & 0 \\ 0 & 0 & 0 & 0 & 0 & 0 \\ 0 & 0 & 0 & 0 & 0 & 0 \end{bmatrix}. \tag{9}$$

The time-dependent elements of matrices $\mathbf{M}(t)$, $\mathbf{K}(t)$ and $\mathbf{C}(t)$ are representing the collections of the parameters given in Eqs. (4) and (5) and can be easily calculated by writing the corresponding equations for the unit cells of corresponding lattices. However, for the sake of clarity, the elements of the mass and stiffness matrices for the left ($\mathbf{M}^{(l)}(t)$, $\mathbf{K}^{(l)}(t)$ and $\mathbf{C}^{(l)}(t)$) and right ($\mathbf{M}^{(r)}(t)$, $\mathbf{K}^{(r)}(t)$ and $\mathbf{C}^{(r)}(t)$) interactions are given in Appendix 1.

2.3. Fourier expansion for time-modulated lattices

In order to apply the plane wave expansion method, where the displacement vector and time-dependent mass and stiffness matrices are expanded into the Fourier series, we assume the modulation of the mass and stiffness matrices as a wave propagation of the velocity $v_m = \frac{\lambda_m}{T_m}$. The terms λ_m and T_m are related to the spatial wavelength and temporal period of modulation, respectively. The mass and stiffness matrices formulated as periodic functions of time with period T_m are expressed as

$$\mathbf{M}(t) = \mathbf{M}(t+T_m), \quad \mathbf{C}(t) = \mathbf{C}(t+T_m), \quad \mathbf{K}(t) = \mathbf{K}(t+T_m), \tag{10}$$

which after Fourier expansion yields the following mass matrices

$$\mathbf{M}(t) = \sum_{q=-\infty}^{\infty} \mathbf{M}_q e^{iq\omega_m t}, \quad \mathbf{M}^{(l)}(t) = \sum_{q=-\infty}^{\infty} \mathbf{M}_q^{(l)} e^{iq\omega_m t}, \quad \mathbf{M}^{(r)}(t) = \sum_{q=-\infty}^{\infty} \mathbf{M}_q^{(r)} e^{iq\omega_m t}, \tag{11}$$

stiffness matrices

$$\mathbf{K}(t) = \sum_{q=-\infty}^{\infty} \mathbf{K}_q e^{iq\omega_m t}, \quad \mathbf{K}^{(l)}(t) = \sum_{q=-\infty}^{\infty} \mathbf{K}_q^{(l)} e^{iq\omega_m t}, \quad \mathbf{K}^{(r)}(t) = \sum_{q=-\infty}^{\infty} \mathbf{K}_q^{(r)} e^{iq\omega_m t}, \tag{12}$$

and the matrix of time-modulated inerter properties

$$\mathbf{C}(t) = \sum_{q=-\infty}^{\infty} \mathbf{C}_q e^{iq\omega_m t}, \quad \mathbf{C}^{(l)}(t) = \sum_{q=-\infty}^{\infty} \mathbf{C}_q^{(l)} e^{iq\omega_m t}, \quad \mathbf{C}^{(r)}(t) = \sum_{q=-\infty}^{\infty} \mathbf{C}_q^{(r)} e^{iq\omega_m t} \tag{13}$$

where frequency of modulation ω_m is related to the temporal period of modulation as $T_m = \frac{2\pi}{\omega_m}$. By considering inverse Fourier transformation, it is easy to obtain the following Fourier coefficients for $\mathbf{M}_q$, $\mathbf{M}_q^{(l)}$, $\mathbf{M}_q^{(r)}$, $\mathbf{K}_q$, $\mathbf{K}_q^{(l)}$, $\mathbf{K}_q^{(r)}$ and $\mathbf{C}_q$, $\mathbf{C}_q^{(l)}$, $\mathbf{C}_q^{(r)}$.

By considering the inverse method explained in [4], the plane wave solution of the time-varying lattice model presented in Eq. (6) can be assumed as

$$\mathbf{u}_n(t) = \mathbf{a}(t) e^{i(-n\mu+\omega t)}, \tag{14}$$

where $\mathbf{a}(t) = \mathbf{a}(t+T_m)$ is the vector of periodic amplitude function in time, $\mu = \lambda_m \kappa$ is the dimensionless wavenumber (while κ is the wavenumber) and ω is frequency of the wave propagation. Now, it can be assumed that the vector of time-depended amplitudes can be expanded into Fourier series with time modulation frequency $\omega_m = 2\pi/T_m$ as

$$\mathbf{a}(t) = \sum_{p=-\infty}^{\infty} \mathbf{a}_p e^{ip\omega_m t}. \tag{15}$$

Adopting the Floquet-Bloch theorem given in [4], the solution for displacement vectors of the interaction can be expressed as

$$\mathbf{u}_{n-1}(t) = \mathbf{a}(t) e^{i(-(n-1)\mu+\omega t)} = e^{i\mu}\mathbf{u}_n(t), \tag{16}$$

$$\mathbf{u}_{n+1}(t) = \mathbf{a}(t) e^{i(-(n+1)\mu+\omega t)} = e^{-i\mu}\mathbf{u}_n(t).$$

Introducing the Eq. (14) into the system of equations given in Eq. (6) leads to the following matrix equation

$$\frac{1}{\omega_0^2}\tilde{\mathbf{M}}(t,\mu)\ddot{\mathbf{u}}_n + \frac{\Omega_m}{\omega_0}\tilde{\mathbf{C}}(t,\mu)\dot{\mathbf{u}}_n + \tilde{\mathbf{K}}(t,\mu)\mathbf{u}_n = \mathbf{0}, \tag{17}$$

where mass, stiffness, and time-modulated inerter property matrices are determined as functions of both time t and the dimensionless wavenumber μ. Finally, the mass, stiffness, and time-modulated inerter matrix are given as

$$\tilde{\mathbf{M}}(t,\mu) = \mathbf{M}(t) + \mathbf{M}^{(l)}(t)e^{i\mu} + \mathbf{M}^{(r)}(t)e^{-i\mu}, \tag{18}$$

$$\tilde{\mathbf{K}}(t,\mu) = \mathbf{K}(t) + \mathbf{K}^{(l)}(t)e^{i\mu} + \mathbf{K}^{(r)}(t)e^{-i\mu},$$

$$\tilde{\mathbf{C}}(t,\mu) = \mathbf{C}(t) + \mathbf{C}^{(l)}(t)e^{i\mu} + \mathbf{C}^{(r)}(t)e^{-i\mu}.$$

Therefore, the dispersion characteristics of the time-space modulated lattice structure can be found by combining the Fourier expansion with the Floquet-Bloch theorem for the displacement vector (Eqs. (14)–(16)), mass, stiffness, and time-modulated inerter matrices (Eqs. (11)–(13)), which then should be introduced into the system of differential equations Eq. (17) in order to obtain the quadratic eigenvalue problem as follows

$$\sum_{q=-\infty}^{\infty} [\Omega + (p-q)\Omega_m]^2 \tilde{\mathbf{M}}_q(\mu)\mathbf{a}_{p-q} - i\Omega_m \sum_{q=-\infty}^{\infty} [\Omega + (p-q)\Omega_m]\tilde{\mathbf{C}}_q(\mu)\mathbf{a}_{p-q} - \sum_{q=-\infty}^{\infty} \tilde{\mathbf{K}}_q(\mu)\mathbf{a}_{p-q} = \mathbf{0}, \tag{19}$$

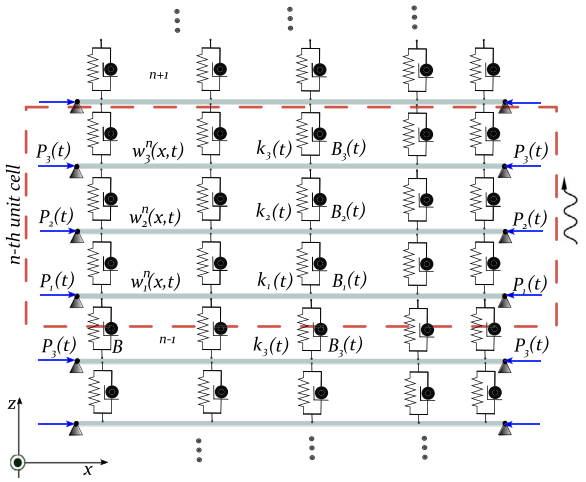

Fig. 3. The inerter-beam based lattice structure and the corresponding UC (red dashed line rectangle). The presented UC contains three simply-supported beams subjected to the time-depended axial loads and coupled through layers of continuously distributed spring-inerter elements. The wavy arrow shows the direction of wave propagation. (For interpretation of the references to colour in this figure legend, the reader is referred to the web version of this article.)

with the dimensionless frequencies $\Omega = \omega/\omega_0$ and $\Omega_m = \omega_m/\omega_0$ and the Fourier coefficients obtained as

$$\tilde{\mathbf{M}}_q(\mu) = \frac{1}{T_m}\int_{-T_m/2}^{T_m/2}\left[\mathbf{M}(t) + \mathbf{M}^{(l)}(t)e^{i\mu} + \mathbf{M}^{(r)}(t)e^{-i\mu}\right]e^{-iq\omega_m t}dt, \tag{20}$$

$$\tilde{\mathbf{K}}_q(\mu) = \frac{1}{T_m}\int_{-T_m/2}^{T_m/2}\left[\mathbf{K}(t) + \mathbf{K}^{(l)}(t)e^{i\mu} + \mathbf{K}^{(r)}(t)e^{-i\mu}\right]e^{-iq\omega_m t}dt,$$

$$\tilde{\mathbf{C}}_q(\mu) = \frac{1}{T_m}\int_{-T_m/2}^{T_m/2}\left[\mathbf{C}(t) + \mathbf{C}^{(l)}(t)e^{i\mu} + \mathbf{C}^{(r)}(t)e^{-i\mu}\right]e^{-iq\omega_m t}dt.$$

The relation Eq. (19) represents a slight generalization of the eigenvalue problem which enables us to study the asymmetric band gaps of time-modulated lattices, where every matrix is a function of the wavenumber μ.

In general case, numbers p and q can take values from minus to plus infinity, but here we adopt a finite number of terms in the Fourier series expansion. In such a truncated expansion, the number of equations given in Eq. (19) can be reduced to the system of $(R+N_r)(2p+1)$ algebraic equations. When taking the value of $p=1$ and $q=2$, the system Eq. (19) is reduced to the following quadratic eigenvalue problem

$$(\Omega^2\mathbf{A}_1 + \Omega\mathbf{A}_2 + \mathbf{A}_3)\mathbf{a} = \mathbf{0}, \tag{21}$$

where Ω and $\mathbf{a}$ are the eigenvalues and eigenvectors of the system, respectively. The matrices $\boldsymbol{A}_1$, $\boldsymbol{A}_2$ and $\boldsymbol{A}_3$ are determined as

$$\mathbf{A}_1 = \begin{bmatrix} \tilde{\mathbf{M}}_0 & \tilde{\mathbf{M}}_{-1} & \tilde{\mathbf{M}}_{-2} \\ \tilde{\mathbf{M}}_1 & \tilde{\mathbf{M}}_0 & \tilde{\mathbf{M}}_{-1} \\ \tilde{\mathbf{M}}_2 & \tilde{\mathbf{M}}_1 & \tilde{\mathbf{M}}_0 \end{bmatrix}, \quad \mathbf{A}_2 = 2\Omega_m \begin{bmatrix} -\tilde{\mathbf{M}}_0 & \mathbf{0} & \tilde{\mathbf{M}}_{-2} \\ -\tilde{\mathbf{M}}_1 & \mathbf{0} & \tilde{\mathbf{M}}_{-1} \\ -\tilde{\mathbf{M}}_2 & \mathbf{0} & \tilde{\mathbf{M}}_0 \end{bmatrix} - i\Omega_m \begin{bmatrix} \tilde{\mathbf{C}}_0 & \tilde{\mathbf{C}}_{-1} & \tilde{\mathbf{C}}_{-2} \\ \tilde{\mathbf{C}}_1 & \tilde{\mathbf{C}}_0 & \tilde{\mathbf{C}}_{-1} \\ \tilde{\mathbf{C}}_2 & \tilde{\mathbf{C}}_1 & \tilde{\mathbf{C}}_0 \end{bmatrix},$$

$$\mathbf{A}_3 = \Omega_m^2 \begin{bmatrix} \tilde{\mathbf{M}}_0 & \mathbf{0} & \tilde{\mathbf{M}}_{-2} \\ \tilde{\mathbf{M}}_1 & \mathbf{0} & \tilde{\mathbf{M}}_{-1} \\ \tilde{\mathbf{M}}_2 & \mathbf{0} & \tilde{\mathbf{M}}_0 \end{bmatrix} - \begin{bmatrix} \tilde{\mathbf{K}}_0 & \tilde{\mathbf{K}}_{-1} & \tilde{\mathbf{K}}_{-2} \\ \tilde{\mathbf{K}}_1 & \tilde{\mathbf{K}}_0 & \tilde{\mathbf{K}}_{-1} \\ \tilde{\mathbf{K}}_2 & \tilde{\mathbf{K}}_1 & \tilde{\mathbf{K}}_0 \end{bmatrix} - i\Omega_m^2 \begin{bmatrix} -\tilde{\mathbf{C}}_0 & \mathbf{0} & \tilde{\mathbf{C}}_{-2} \\ -\tilde{\mathbf{C}}_1 & \mathbf{0} & \tilde{\mathbf{C}}_{-1} \\ -\tilde{\mathbf{C}}_2 & \mathbf{0} & \tilde{\mathbf{C}}_0 \end{bmatrix}. \tag{22}$$

The solution of the eigenvalue problem given in Eq. (21) can provide the dispersion characteristics of the proposed time-modulated inerter-based lattices.

3. The inerter-beam based lattice structure

The second example of the PL model analyzed here is based on an array of parallel elastic beams mutually connected through the layers of continuously distributed springs and inerter elements as shown in Fig. 3. The Euler-Bernoulli beam model is adopted with simply-supported boundary conditions at each end. In order to achieve the time-modulated mass and stiffness properties in the proposed lattice, each beam is subjected to time-dependent axial load and connected through the time-dependent spring and inerter elements in the connecting layers. In a similar manner as before, it is considered that

the periodically repeating unit cell of the proposed lattice consists of $R = 3$ coupled beams as highlighted by a red dashed rectangular line in Fig. 3. The end conditions of a finite lattice structure chain are assumed to be of the Born-Karman type in order to remove the reflection of the waves at boundaries. The governing equation of motion for the Euler-Bernoulli beam with simply-supported boundary conditions and constant material parameters is derived in [43], Ch 3. However, the model of the lattice presented here is based on multiple Euler-Bernoulli beams coupled through time-modulated springs and inerters and applied time-varying axial load. Therefore, the presented model is an extension of the classical models of uni-directional waveguides based on coupled beam systems with constant parameters.

The governing equations of motion of the phononic waveguide for the nth UC are given in the dimensionless form as

$$\frac{\partial^4 w_1^n}{\partial \xi^4} + \tilde{K}_1(\tau)(w_1^n - w_2^n) + \tilde{K}_3(\tau)(w_1^n - w_3^{n-1}) + \ddot{w}_1^n + \tilde{P}_1(\tau)\frac{\partial^2 w_1^n}{\partial \xi^2} + \tag{23}$$

$$\tilde{B}_1(\tau)(\ddot{w}_1^n - \ddot{w}_2^n) + \tilde{B}_3(\tau)(\ddot{w}_1^n - \ddot{w}_3^{n-1}) + \dot{\tilde{B}}_1(\tau)(\dot{w}_1^n - \dot{w}_2^n) + \dot{\tilde{B}}_3(\tau)(\dot{w}_1^n - \dot{w}_3^{n-1}) = 0,$$

$$\frac{\partial^4 w_2^n}{\partial \xi^4} + \tilde{K}_1(\tau)(w_2^n - w_1^n) + \tilde{K}_2(\tau)(w_2^n - w_3^n) + \ddot{w}_2^n + \tilde{P}_2(\tau)\frac{\partial^2 w_2^n}{\partial \xi^2} + \tag{24}$$

$$\tilde{B}_1(\tau)(\ddot{w}_2^n - \ddot{w}_1^n) + \tilde{B}_2(\tau)(\ddot{w}_2^n - \ddot{w}_3^n) + \dot{\tilde{B}}_1(\tau)(\dot{w}_2^n - \dot{w}_1^n) + \dot{\tilde{B}}_2(\tau)(\dot{w}_2^n - \dot{w}_3^n) = 0,$$

$$\frac{\partial^4 w_3^n}{\partial \xi^4} + \tilde{K}_2(\tau)(w_3^n - w_2^n) + \tilde{K}_3(\tau)(w_3^n - w_1^{n+1}) + \ddot{w}_3^n + \tilde{P}_3(\tau)\frac{\partial^2 w_3^n}{\partial \xi^2} + \tag{25}$$

$$\tilde{B}_2(\tau)(\ddot{w}_3^n - \ddot{w}_2^n) + \tilde{B}_3(\tau)(\ddot{w}_3^n - \ddot{w}_1^{n+1}) + \dot{\tilde{B}}_2(\tau)(\dot{w}_3^n - \dot{w}_2^n) + \dot{\tilde{B}}_3(\tau)(\dot{w}_3^n - \dot{w}_1^{n+1}) = 0,$$

where $w_r^n = w_r^n(\xi, \tau)$ is the dimensionless displacements of the rth beam ($r = 1, 2, 3$), in the nth unit cell. The terms $\tilde{K}_r(\tau)$, $\tilde{B}_3(\tau)$, and $\tilde{P}_r(\tau)$ are representing the time-modulated parameters related to stiffness and inerter properties of coupling layers and time-varying axial load, respectively. The dimensionless time is adopted as $\tau = \omega_0 t$, $\omega_0 = \frac{1}{L^2}\sqrt{\frac{EI}{\rho A}}$ and the space coordinate as $x = \xi L$.

By introducing the Galerkin method for the discretization of the governing partial differential equations, we can assume a solution in the following manner

$$w_r^n(\xi, \tau) = \sum_{i=1}^{N} \phi_i(\xi) q_{ri}^n(\tau) = \mathbf{l}(\xi)\mathbf{q}_r^n(\tau), \quad r = 1, ., R, \tag{26}$$

where $\mathbf{l} = \mathbf{l}(\xi)$ and $\mathbf{q}_r^n = \mathbf{q}_r^n(\tau)$ are vectors with components $\phi_i(\xi)$ and $q_{ri}^n(\tau)$. The mode shape functions $\phi_i(\xi)$ for simply-supported boundary conditions of the single Euler-Bernoulli beam are adopted from Zhang et al. [44]. In this study, we adopt $N = 5$ Galerkin terms to discretize the governing equations of motion. Such discretized differential equations with time functions $q_{ri}^n(\tau)$ will be used to later define the corresponding eigenvalue problem.

Introducing Eq. (26) into the system of equations Eqs. (23)–(25) and applying the mode shape orthogonality condition, we can obtain the corresponding matrix equation in the similar form as in Eq. (6), which yields

$$\mathbf{M}(\tau)\ddot{\mathbf{q}}_n + \mathbf{C}(\tau)\dot{\mathbf{q}}_n + \mathbf{K}(\tau)\mathbf{q}_n + \tag{27}$$

$$\mathbf{M}^{(l)}(\tau)\ddot{\mathbf{q}}_{n-1} + \mathbf{C}^{(l)}(\tau)\dot{\mathbf{q}}_{n-1} + \mathbf{K}^{(l)}(\tau)\mathbf{q}_{n-1} + \mathbf{M}^{(r)}(\tau)\ddot{\mathbf{q}}_{n+1} + \mathbf{C}^{(r)}(\tau)\dot{\mathbf{q}}_{n+1} + \mathbf{K}^{(r)}(\tau)\mathbf{q}_{n+1} = \mathbf{0},$$

After applying the Floquet-Bloch theorem on the above equations, a system of ordinary differential equations for the nth cell is obtained in the following form

$$\tilde{\mathbf{M}}(\tau, \mu)\ddot{\mathbf{q}}_n + \tilde{\mathbf{C}}(\tau, \mu)\dot{\mathbf{q}}_n + \tilde{\mathbf{K}}(\tau, \mu)\mathbf{q}_n = \mathbf{0}, \tag{28}$$

or in the expended form,

$$\begin{bmatrix} \tilde{\mathbf{M}}_1 & -\tilde{B}_1\mathbf{A}_G & -\tilde{B}_3\mathbf{A}_G e^{i\mu} \\ -\tilde{B}_1\mathbf{A}_G & \tilde{\mathbf{M}}_2 & -\tilde{B}_2\mathbf{A}_G \\ -\tilde{B}_3\mathbf{A}_G e^{-i\mu} & \tilde{B}_2\mathbf{A}_G & \tilde{\mathbf{M}}_3 \end{bmatrix} \begin{bmatrix} \ddot{\mathbf{q}}_1 \\ \ddot{\mathbf{q}}_2 \\ \ddot{\mathbf{q}}_3 \end{bmatrix}^n + \begin{bmatrix} \tilde{\mathbf{C}}_1 & -\dot{\tilde{B}}_1\mathbf{A}_G & -\dot{\tilde{B}}_3\mathbf{A}_G e^{i\mu} \\ -\dot{\tilde{B}}_1\mathbf{A}_G & \tilde{\mathbf{C}}_2 & -\dot{\tilde{B}}_2\mathbf{A}_G \\ -\tilde{B}_3\mathbf{A}_G e^{-i\mu} & \dot{\tilde{B}}_2\mathbf{A}_G & \tilde{\mathbf{C}}_3 \end{bmatrix} \begin{bmatrix} \dot{\mathbf{q}}_1 \\ \dot{\mathbf{q}}_2 \\ \dot{\mathbf{q}}_3 \end{bmatrix}^n + \tag{29}$$

$$\begin{bmatrix} \tilde{\mathbf{K}}_1 & -\tilde{K}_1\mathbf{A}_G & -\tilde{K}_3\mathbf{A}_G e^{+i\mu} \\ -\tilde{K}_1\mathbf{A}_G & \mathbf{K}_2 & -\tilde{K}_2\mathbf{A}_G \\ -\tilde{K}_3\mathbf{A}_G e^{-i\mu} & \tilde{K}_2\mathbf{A}_G & \mathbf{K}_3 \end{bmatrix} \begin{bmatrix} \mathbf{q}_1 \\ \mathbf{q}_2 \\ \mathbf{q}_3 \end{bmatrix}^n = \begin{bmatrix} \mathbf{0} \\ \mathbf{0} \\ \mathbf{0} \end{bmatrix}.$$

where

$$\tilde{\mathbf{M}}_r(\tau) = (1 + \tilde{B}_r(\tau) + \tilde{B}_{r-1}(\tau))\mathbf{A}_G,$$

Table 1
The parameters for the time history simulations.

Type of model	The excitation period T_{ex}	The simulation period T_{sim}	The increment h
Discrete models	200	1000	1×10^{-1}
Structural model	30	90	1×10^{-3}

$$\tilde{\mathbf{K}}_r(\tau) = \mathbf{B}_G + (\tilde{K}_r(\tau) + \tilde{K}_{r-1}(\tau))\mathbf{A}_G + \tilde{P}_r(\tau)\mathbf{C}_G,$$

$$\tilde{\mathbf{C}}_r(\tau) = (\dot{\tilde{B}}_r(\tau) + \dot{\tilde{B}}_{r-1}(\tau))\mathbf{A}_G, \quad r = 1, 2, 3.$$

The matrices obtained by applying the Galerkin procedures are given as

$$\mathbf{A}_G = \int_0^1 \mathbf{l}^T(\xi)\mathbf{l}(\xi)d\xi, \quad \mathbf{B}_G = \int_0^1 \mathbf{l}^T(\xi)\frac{d^4\mathbf{l}(\xi)}{d\xi^4}d\xi, \quad \mathbf{C}_G = \int_0^1 \mathbf{l}^T(\xi)\frac{d^2\mathbf{l}(\xi)}{d\xi^2}d\xi.$$

To determine the dispersion characteristic of the system and find asymmetric band gaps the quadratic eigenvalue problem should be defined from Eq. (28) and then solved by following the methodology discussed in the previous section.

4. Dispersion and uni-directional wave propagation analysis

The aim of the numerical study is to verify the applicability of the method proposed above for performing the dispersion analysis of the time-modulated periodic elastic lattices. The cases with and without local resonators given as one-dimensional chains with inerters are considered. Moreover, uni-directional wave propagation is observed based on the solution of a system of equations using the finite difference method (see **Appendix 3**). In the first part, dispersion curves are obtained based on the Eq. (21) and corresponding matrices from Eq. (22). It should be noted that the masses M and m in the system are considered to be constant in time while the properties of springs and inerters connecting adjacent masses are time-modulated according to the periodic functions given by Eqs. (4) and (5) with the period of the time modulation T_m. In the second part, the same type of analysis is performed for a UC of an array of elastic beams connected through time-modulated springs and inerters and with constant mass properties of the beams. Additionally, periodic time-varying axial loads are applied to each of the beams, thus modulating their stiffness properties. We note that in the given examples mass matrices are time-dependent functions due to the modulation of the inerter properties. Therefore, we can state that simultaneous modulation of stiffness and mass properties occurs in the observed one-dimensional chains. For the time history analysis, we adopt the dimensionless time, where $\tau = \omega_0 t$. Time excitation period T_{ex} and simulation time period T_{sim} used in time response simulations for discrete and discrete-continuous structural models of PL and LRL systems are given in Table 1.

4.1. Time-modulated one-dimensional mass-spring-inerter system

Here, we study a general case of the one-dimensional chain with UC having $R = 3$ masses connected to the ground and to the adjacent UCs through springs and inerters. First, only the stiffness properties of springs are modulated and then a simultaneous modulation of inerters and springs is conducted. Let us first consider the solutions obtained by taking $\mu \in [-\pi, \pi]$ which for the non-modulated chain yields three bands given by Fig. 4a with three band gaps including the zero frequency band gap induced by ground springs. If $P = 1$ terms in the Fourier expansion are introduced, according to the formula $(R + N_r)(2P + 1)$ this will lead to nine dispersion branches (where $N_r = 0$ for the lattice without internal resonators) that are plotted in terms of the dimensionless frequency. In Fig. 4b one can observe many crossings for certain values of the wavenumber as well as folding of dispersion branches at the edges of the first Brillouin zone. Three families of curves can be observed, which are parallel to each other and separated by the modulation frequency Ω_m. Next, the filtering method based on the weighting and threshold process is applied based on the procedure described in [15] in order to identify fundamental branches associated with the component of a fundamental plane wave among the given three families of curves. The number of fundamental branches is directly related to the number of dispersion curves in the lattice without time-modulated properties. In general, the weighting and threshold procedure involves selection of the branch that corresponds to the fundamental plane wave (the one carrying the most of the energy), by identifying the eigenvector corresponding to the fundamental plane wave and using its values as a threshold to which all other values are compared. This process eliminates from the final band diagram all the values that exceed the threshold ones. The color legends that are given in each figure show that the fundamental branches correspond to the values of the normalized eigenvectors whose maximal amplitude is equal to one. This process leads to showing only the fundamental branches characterized by a high-pass cut-off at the frequency around $\Omega = 1$ at $\mu = 0$ due to the ground spring stiffness, and the low-pass cut-off at $\mu = \pm\pi$, Fig. 4c. Moreover, one can observe the asymmetry between the band gaps on the left and the right-hand side of the center of the Brillouin zone is caused by the stiffness modulation of springs. This is in line with the results obtained for the similar time-modulated stiffness periodic lattice system without inerter elements observed in [15]. Such asymmetric band structure leads

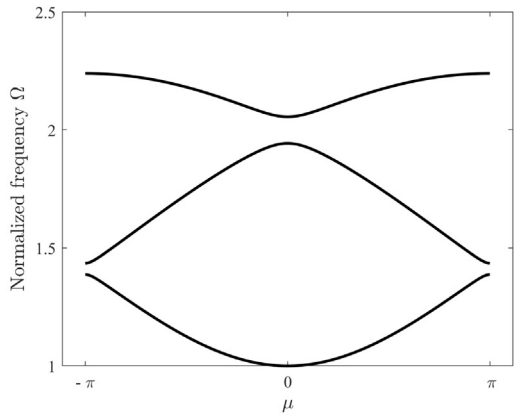

(a) Dispersion curves of the non-modulated lattice.

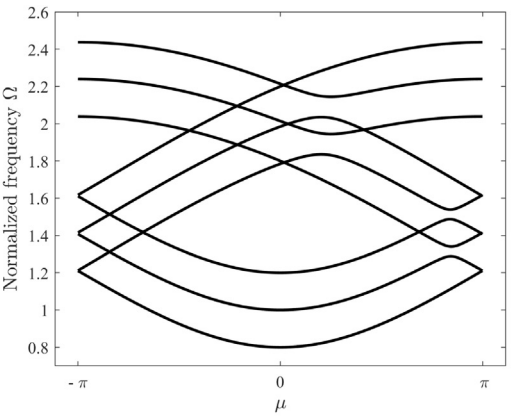

(b) Dispersion curves of the time-modulated lattice.

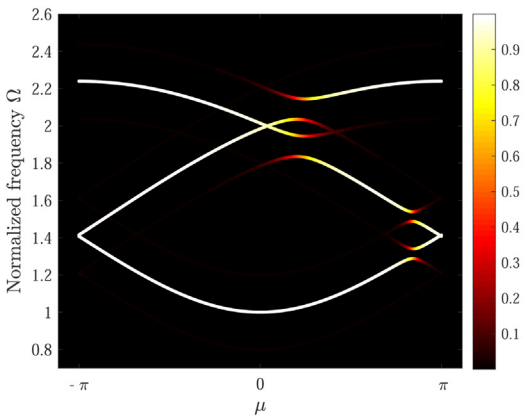

(c) Fundamental branches of the time-modulated lattice.

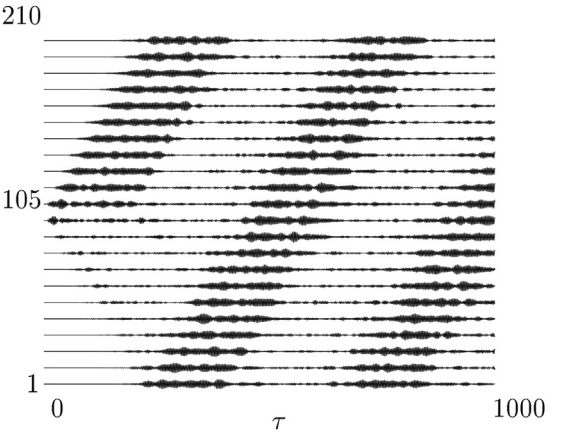

(d) Time response to harmonic excitation of a lattice.

Fig. 4. The phononic structure with time-varying stiffness properties. The excitation frequency adopted from the asymmetric band-gap to show the uni-directional wave propagation in the time response analysis is $\Omega = 1.9$.

to the ability of periodic lattices to support uni-directional wave propagation. Since frequency within one of the band gaps is defined either by negative or positive wavenumber, the wave can propagate only in the backward or forward direction. Therefore, for frequencies that belong to the asymmetric band gaps, the lattices with time-modulated properties behave as a non-reciprocal medium after breaking the time-reversal symmetry. The influence of these properties on wave motion in finite lattices can be illustrated through the uni-directional wave propagation for spatio-temporal modulation of the lattice. The same values of parameters are used in the dispersion analysis. The transient response of the chain is measured for the central mass excited at the frequency $\Omega = 1.9$ of the asymmetric band gap lying on the negative slope dispersion branch (see Fig. 4c). This will allow only the propagation of wave modes with positive group velocities i.e. in the forward lattice direction $+x$. The total number of 70 UCs or 210 masses in the lattice is adopted with the modulation period $\lambda_m = 3a$. Born-Karman boundary conditions are used to prevent reflections at the edges of the lattice. The finite difference method is applied to numerically integrate the differential equations with the time step $h = 1 \times 10^{-1}$. Figure 4d shows the resulting displacements along the chain against the non-dimensional time τ revealing the strongly asymmetric behavior of the displacement field due to the fact that most of the wave motion energy is carried by the waves propagating in the forward lattice direction. When the primary wavefront reaches one edge of the chain it appears again on the other edge due to the adopted Born-Karman boundary conditions. One can also observe waves with a frequency different from the picked frequency Ω propagating in both directions but having much smaller amplitudes and group velocities different from the primary wave.

As mentioned previously in the text, not only the stiffness properties can be modulated in time. If we apply the periodic time-modulation of the inerters, the mass properties can also vary in time. Therefore, time-modulated inerters can serve as another mechanism to achieve uni-directional wave propagation in periodic structures. For that purpose, we adopt the same stiffness and mass properties as well as time-periodic modulation functions like in the previous case but with the following inerters parameters $s = 0.1$, $\epsilon_g = 0.2$, $\rho_m = 0.1$ and $\rho_{gm} = 0.13$. At the first sight, the dispersion curves in Fig. 5a, b, and c

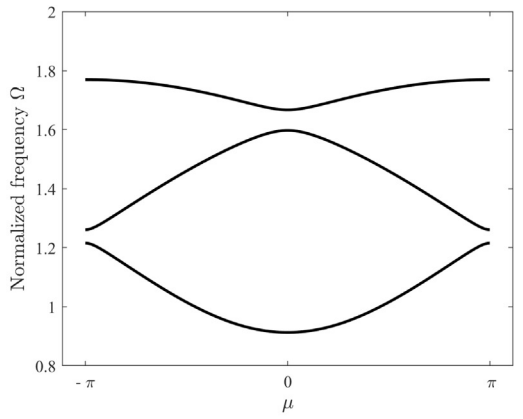

(a) Dispersion curves of the non-modulated lattice.

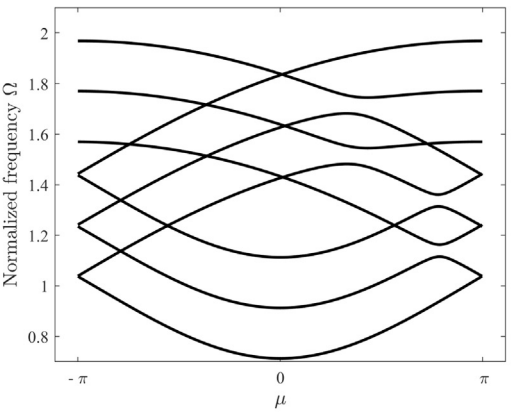

(b) Dispersion curves of the time-modulated lattice.

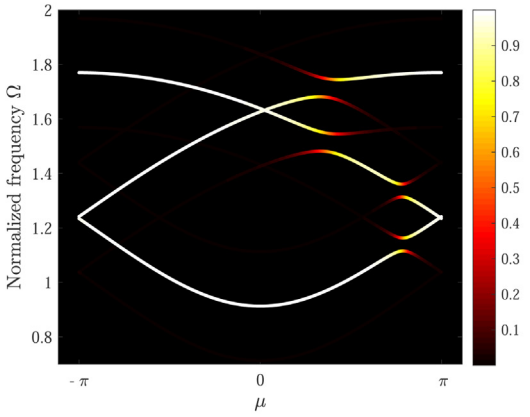

(c) Fundamental branches of the time-modulated lattice.

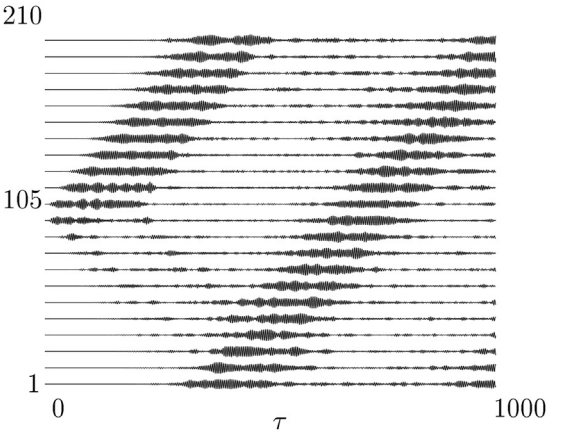

(d) Time response to harmonic excitation of a lattice.

Fig. 5. The phononic structure with time-varying inerter and stiffness properties. The excitation frequency adopted from the asymmetric band-gap to show the uni-directional wave propagation in the time response analysis is $\Omega = 1.52$.

look the same as those in Fig. 4. However, a closer look reveals that in the configuration with inerters the asymmetric band gaps are shifted to lower frequencies. Moreover, when comparing the main dispersion branches in Fig. 5c and Fig. 4c, it can be observed that in the case with time-modulated inerters edges of the first and the second asymmetric band gaps are shifted to the left while those of the third and fourth band gap is shifted to the right on the wavenumber axis. Such a unique behavior of lattices with time-modulated springs and inerters was not observed earlier in the literature. This shows a high potential for inerters to be used as band gap tuning devices in elastic periodic structures with time modulation of mass and stiffness properties. Further, Fig. 5d displays uni-directional wave propagation for the excitation frequency $\omega_m = 1.52$ within the third asymmetric band gap lying on the negative slope dispersion branch (Fig. 5c). Here, in the same way, as in the previous case, the main wave motion energy is supported by the waves propagating in the forward direction, while some of the waves of different frequencies and smaller amplitudes are propagating in both directions. Here, for the period of $T_{sim} = 1000$, the traveling wave was able to reach the boundary of the chain just once while it reached the boundary twice in the preceding case. This can be attributed to the fact that the frequency of the wave is lower in the second case.

4.2. Time-modulated one-dimensional mass-spring-inerter system with local resonators

In the same context we can analyse discrete mass-spring-inerter lattices with internal resonators. It is well known that one-dimensional non-modulated elastic metamaterials can be represented by simple mass-spring periodic lattices with local resonators, known as the acoustic metamaterials. One of the main characteristic of such systems are low frequency band gaps. Depending on the properties of local resonators, band gaps of locally resonant origin are often bounded by flat bands. If we introduce the time-modulated stiffness properties, dispersion characteristic can be changed and the non-reciprocal behavior can occur in such system. Therefore, one-dimensional lattice is considered, with the UC consisting of $N_r = 3$ inner resonators and $R = 3$ outer masses connected to the ground and to the adjacent masses through springs and inerters, as it is shown on Fig. 2b. Unless stated otherwise, the following system parameters are used in simulations: $\Omega_m = 0.2$, $\beta_m = 0.15$,

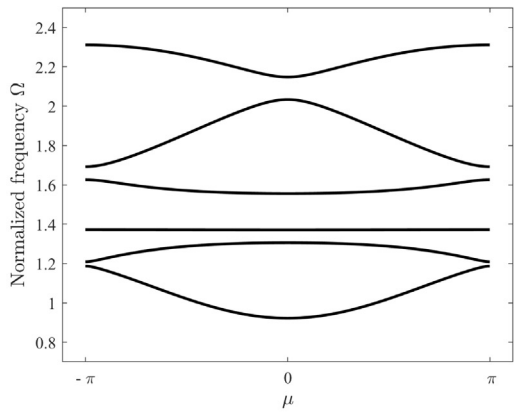

(a) Dispersion curves of the non-modulated lattice.

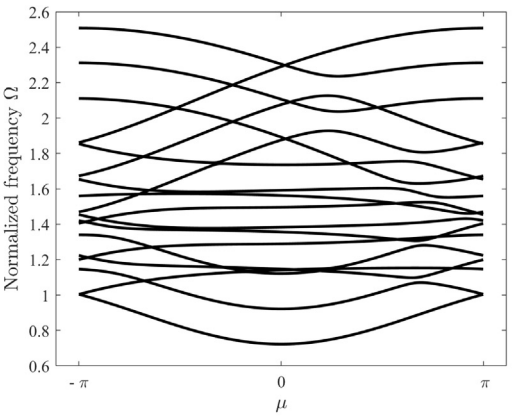

(b) Dispersion curves of the time-modulated lattice.

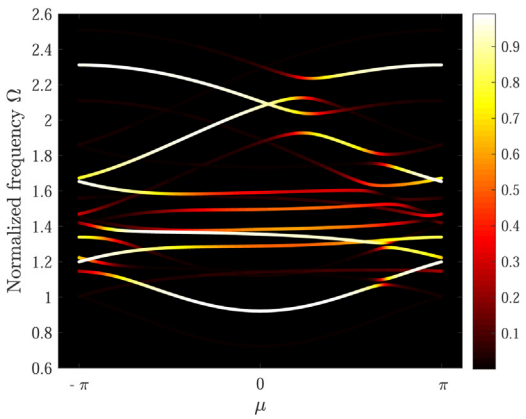

(c) Fundamental branches of the time-modulated lattice.

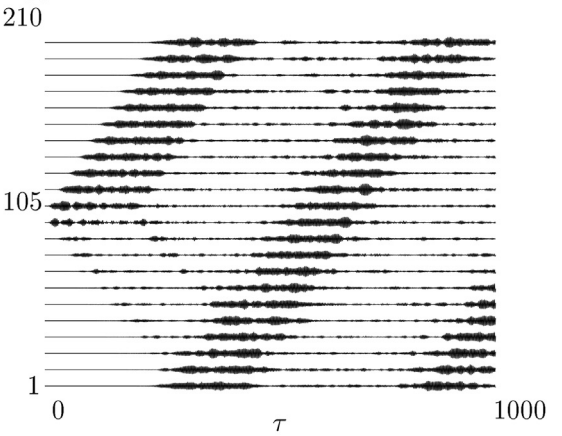

(d) Time response to harmonic excitation of a lattice.

Fig. 6. The local resonant structure with time-varying stiffness properties. The excitation frequency adopted from the asymmetric band-gap to show the uni-directional wave propagation in the time response analysis is $\Omega = 2.01$.

$\gamma_g = 1$, $b = 0.1$, $\theta_m = 0.15$ and $\xi_R = 0.2$. Figure 6a shows the band structure of the non-modulated lattice if the influence of the inerters was to be neglected. Six dispersion branches with five band gaps (plus the zero frequency band gap induced by ground springs) can be identified in the band structure. Narrow band gaps that appear at the edges and in the middle of the Brillouin zone can be characterized as Bragg type band gaps due to the nature of the bounding bands. However, Fig. 6b shows dispersion branches of the stiffness-modulated lattice obtained for the $P = 1$ terms in the the Fourier expansion and whose number can be calculated according to the formula $(R + N_r)(2P + 1)$. Many band crossings and closings of dispersion curves can be observed within the span and at the edges of the first Brillouin zone. Better understanding of the dispersion characteristic can be obtained from Fig. 6c after performing the weighting and threshold process. Here, the asymmetric band gaps can be viewed for positive wavenumbers. The structure of these band gaps is much different than those of the lattice without resonators. The asymmetric band gaps that appear in the lower frequency branches are very narrow while those at higher frequencies are wider. Uni-directional wave propagation is investigated for the finite lattice (with 70 UCs) in Fig. 6d by imposing the excitation frequency $\Omega = 2.01$, which lies within the higher frequency asymmetric band gap. Only the displacement amplitudes of the outer masses are analyzed. The primary wave travels in the $+x$ direction, which is the characteristic of modes with positive group velocities. Here, some "leaking" of waves with frequencies and amplitudes different from the ones of the primary wave can also be noticed traveling in both directions.

Much different behavior can be noticed in the lattices with local resonators and included inerter elements. The following properties of inerters are used in numerical simulations: $\Omega_m = 0.2$, $\beta_m = 0.15$, $\gamma_g = 1$, $b = 0.1$, $\theta_m = 0.15$, $s = 0.1$, $\epsilon_g = 0.2$ and $\xi_R = 0.2$. Let us first compare the band structures of the non-modulated lattices $\Omega_m = 0$ without the inerter elements (Fig. 6a) and with the inerter elements (Fig. 7a). One can notice an obvious shifting of dispersion branches and band gaps to lower frequencies due to the introduced inerters. After the simultaneous time-modulation of stiffness and inertia properties is applied, the dispersion characteristic of the lattice is significantly changed. Figure 7b shows many crossings and foldings of dispersion branches within and at the edges of the first Brillouin zone. A much better picture can be obtained after

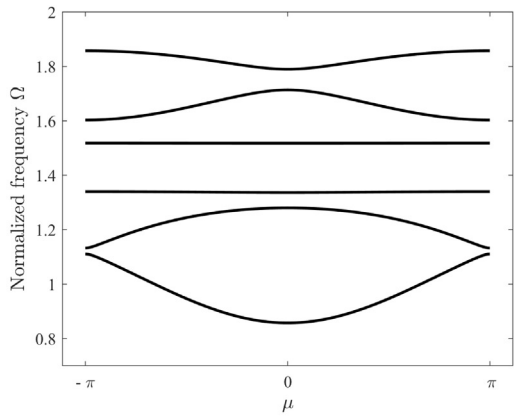

(a) Dispersion curves of the non-modulated lattice.

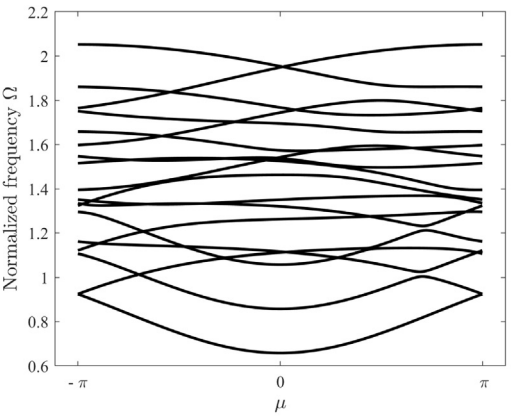

(b) Dispersion curves of the time-modulated lattice.

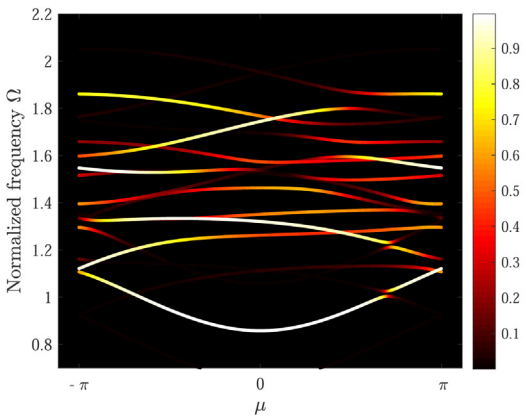

(c) Fundamental branches of the time-modulated lattice.

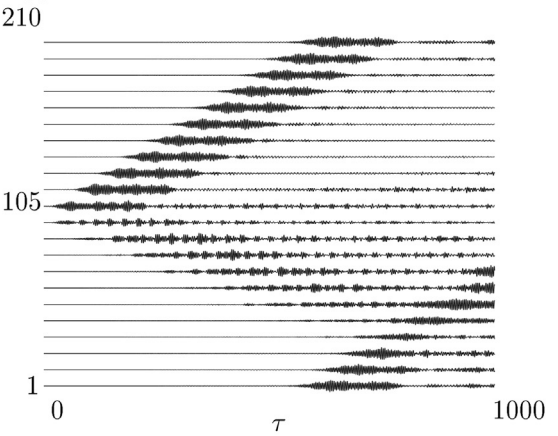

(d) Time response to harmonic excitation of a lattice.

Fig. 7. The local resonant structure with time-varying inerter and stiffness properties. The excitation frequency adopted from the asymmetric band-gap to show the uni-directional wave propagation in the time response analysis is $\Omega = 1.7$.

performing the weighting and threshold process that leaves only the fundamental branches, Fig. 7c. A similar structure of the asymmetric band gaps can be observed in this configuration as well, but at much lower frequencies due to the introduced inerters. Note that some branches are more faded while some new ones appear when compared to those in the configuration without the inerters as a result of the weighting process. Finally, to demonstrate the uni-directional wave propagation we apply the following frequency of excitation $\Omega = 1.7$ in the finite chain with 70 UCs and analyze only the displacement amplitudes of the outer masses. The spatial profile in Fig. 7d indicates the one-way propagation of the primary wave in the positive direction $+x$. However, it can be noticed that a small portion of wave energy travels to the opposite direction of the main exciting wave, which can be attributed to the fact that additional resonators can store the part of wave energy. Moreover, the excitation frequency should be chosen carefully within the asymmetric band gap which is not well-formed due to the existence of extended fading branches Fig. 7c. Despite these differences, the presented results indicate accurate predictions of asymmetric band gaps based on dispersion and Bloch wave propagation analysis when simultaneous modulation of stiffness and inerter properties is involved.

4.3. Time-modulated inerter-beam based lattice

Upon investigation of the discrete lattice systems with inerters, we now observe the inerter-beam based lattice with time-varying periodic loads applied at beam ends. The Bloch wave propagation analysis of a similar non-modulated system in the configuration without inerters was previously studied in [45]. In the literature, usually, some external fields that involve complicated setups are used to modulate the stiffness properties of materials. Here, we modulate the stiffness properties in a purely mechanical way by applying simple loads at beam ends given as a compressive periodic axial force. After discretization of the governing equations of motions, Mathieu-Hill-type differential equations are obtained for the axially loaded beam system. This enables us to perform the same Bloch-based dispersion analysis of the UC as in the case of discrete lattices. It is assumed that the wave propagates only in the bending direction of the beams. Next, the UC with three

simply supported beams (see Fig. 2 for details) is considered, which are connected with the neighboring beams and UCs through layers of continuously distributed springs and inerters. The following system parameters are used in simulations unless otherwise stated: $\Omega_m = 2$, $\beta_m = 0.2$, $\epsilon = 0.1$, $\delta = 0.1$, $k_0 = 100$, $B_0 = 0.1$, and $P_0 = 0.2$.

Figure 8 a shows the band structure of a UC of the non-modulated inerter-beam lattice with $R \times N$ number of dispersion branches, where $R = 3$ is the number of beams and $N = 5$ is the number of terms (modes) adopted in the Galerkin approximation. A wide frequency range was analyzed and five sets of dispersion branches separated by large band gaps were observed. Each set contains three phononic-like dispersion branches separated by narrow Bragg gaps. For example, the set of dispersion branches at the lowest frequency can be easily retained if only one term is considered in the Galerkin approximation with the band structure of the form similar to those of the non-modulated mass-spring lattice. Here, one can also notice that the zero band gap appears similar to the one in the grounded mass-spring lattice, where now the beam ends conditions play the same role. This also indicates that large band gaps in between the sets of dispersion branches could be induced by the beam's boundary conditions. Further, Fig. 8b shows many dispersion branches obtained when $P = 1$ terms in the Fourier expansion are adopted. All these branches are located around the fundamental modes within the mentioned sets of dispersion branches but because of the narrow passbands and wide frequency range, they can be viewed only as tick lines. However, a closer look will show many crossings and foldings between the dispersion curves. The asymmetric band gaps with respect to the center of the Brillouin can be observed in Fig. 8c obtained from the fundamental modes after the weighting procedure is performed. However, the asymmetric band gaps are not located in the same half of the Brillouin zone. More precisely, in the lower frequency branches, they can be observed only for the positive wavenumbers while in higher frequency modes they are located in the negative half of the Brillouin zone for lower (closer to the center) as well for higher (closer to the edges) values of the wave-number. The non-reciprocal behavior of the proposed lattice for the frequencies within the asymmetric band gaps can be examined based on the spatial-temporal modulation due to the applied harmonic load on beams and the transient response of the system. Finally, the finite lattice (with 50 UCs) is considered by imposing the excitation frequency $\Omega = 18.4$ within the lower frequency asymmetric band gap (Fig. 9). Here, the displacement amplitudes for each beam are considered at the position $0.4L$. It can be observed that the primary wave travels in the $-x$ direction indicating that only negative group velocities are allowed for this band gap. Similar to the discrete lattices, one can notice that some waves excited at a different frequency and have a smaller amplitude than the primary wave are traveling in both directions. It should be noted that the transient response is consistent with the Bloch-based dispersion analysis used to predict wavenumbers and group velocities. Note that in this case we also have the propagation of some waves in the direction opposite to the direction of the main exciting wave. This wave energy leaking depends on the adopted excitation frequency and its position within the asymmetric band gap.

5. Topological properties of the wave dispersion in inerter-based lattice

Topological characterization and bulk-edge correspondence

Here, we only investigate the topological properties of a one-dimensional time-modulated material given as a discrete three-mass-spring phononic lattice with grounded springs. We consider both the time-modulation of spring and inerter properties in the form of T_m periodic functions of time, while masses are assumed to be constant. The adopted system is similar to those studied in [46] except that here the inerter elements and grounded springs on each of the masses within the UC are introduced. The main purpose of this section is to study the existence of topologically protected one-way edge modes based on the bulk-edge correspondence and quantify their time evolution through topologically invariant Chern number. Based on the principle of bulk-edge correspondence one can locate the frequencies of the edge modes and visualize them. The evolution of the frequency spectrum for the finite time-modulated lattice composed of 30 UCs is computed over the first period and for the fixed-chain boundary conditions and presented in Fig. 10. The following modulation parameters are adopted in simulations $\beta_m = 0.15$, $\beta_{gm} = 0.5$, $\gamma_g = 0.3$, $s = 0.01$, $\rho_m = 0.01$, as well as the modulation frequency $\Omega_m = 0.2$. It should be noted that for convenience the ground inerter is neglected in this analysis while for other inerters only a small values of inerter parameter s is adopted. Besides the two main frequency band gaps, one can also observe a zero band gap ranging from the zero frequency to the lowest frequency of the first dispersion branch, which is generated due to the introduced ground springs. However, only the two main higher frequency band gaps are crossed by the eigenfrequencies of edge states spanning the certain range at approximately $0.2T_m$ (see the magnified diagram in Fig. 10b for details) for the first band gap and around $0.96T_m$ for the second band gap (Fig. 10a). To verify the existence of these edge modes in space, six different points are chosen from the frequency spectrum 10 a. Bulk modes are highlighted in green for two points, before and after the first band gap (Fig. 10c and d), while the right (Fig. 10e) and the left (Fig. 10f) edge modes are given in black and red color, respectively. The other two edge modes can be obtained by plotting the real part of the eigenmodes for the corresponding frequency positions from the frequency spectrum, which is presented in Fig. 10b (denoted by triangles colored in magenta and cyan). The localization of displacement amplitudes at the boundaries of the lattice for the chosen edge mode frequencies is clear and consistent with the frequency spectrum analysis.

It is well known that the nonzero Chern number underpins the topological edge states. In [46], the authors proved the adiabatic theorem for time-modulated elastic systems and provided the conditions for which the eigenvalue remains non-degenerate. This condition requires a sufficiently small modulation frequency. However, to quantify the tilting of wave dispersion bands they used the topologically invariant Chern number in its "numerically gauge-invariant" form, which does

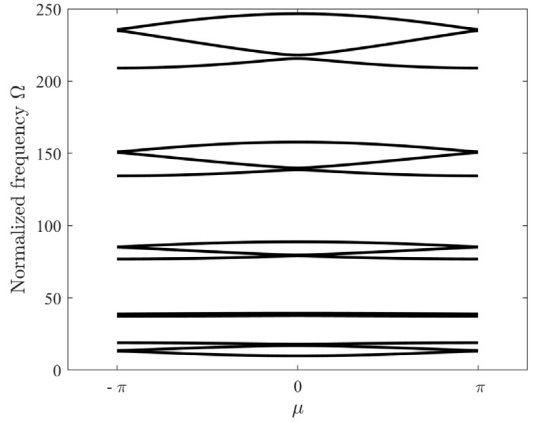

(a) Dispersion curves of the non-modulated lattice.

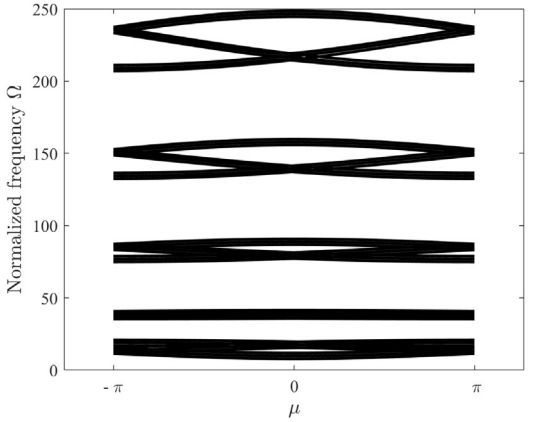

(b) Dispersion curves of the time-modulated lattice.

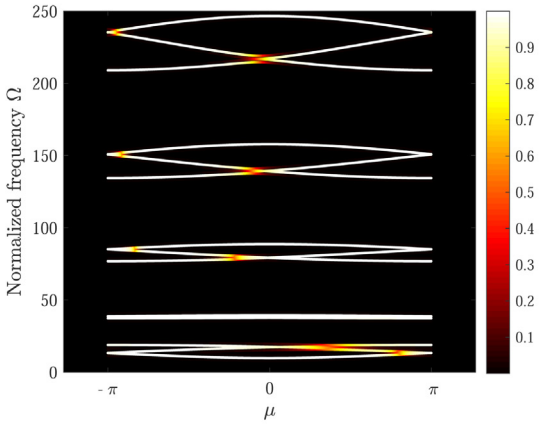

(c) Fundamental branches of the time-modulated lattice.

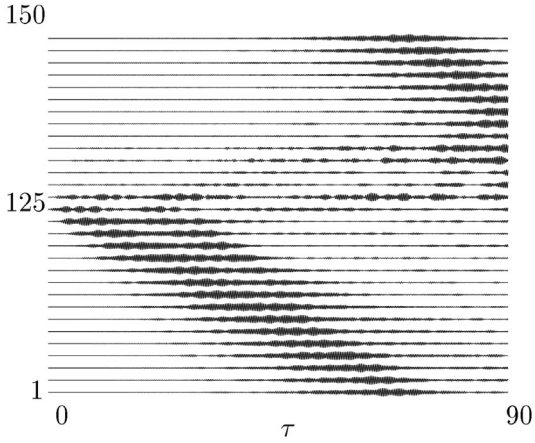

(d) Time response to harmonic excitation of a lattice.

Fig. 8. The inerter-beam based lattices subjected to time-varying axial load. The number of adopted terms in Galerkin approximation is $N = 5$. The excitation frequency adopted from the asymmetric band gap to show the uni-directional wave propagation in the time response analysis is $\Omega = 18.4$.

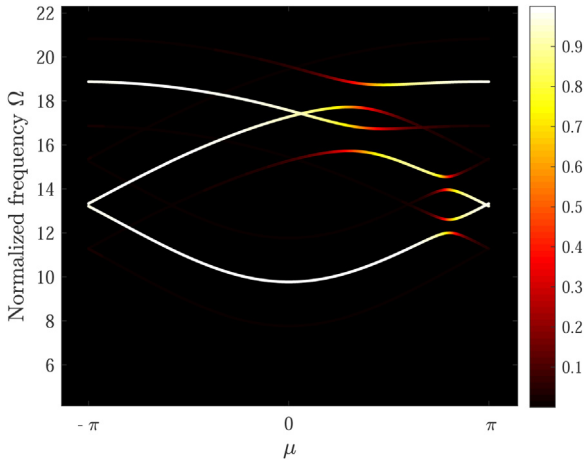

Fig. 9. The magnified first three fundamental bands from Fig. 8c showing asymmetric band gaps.

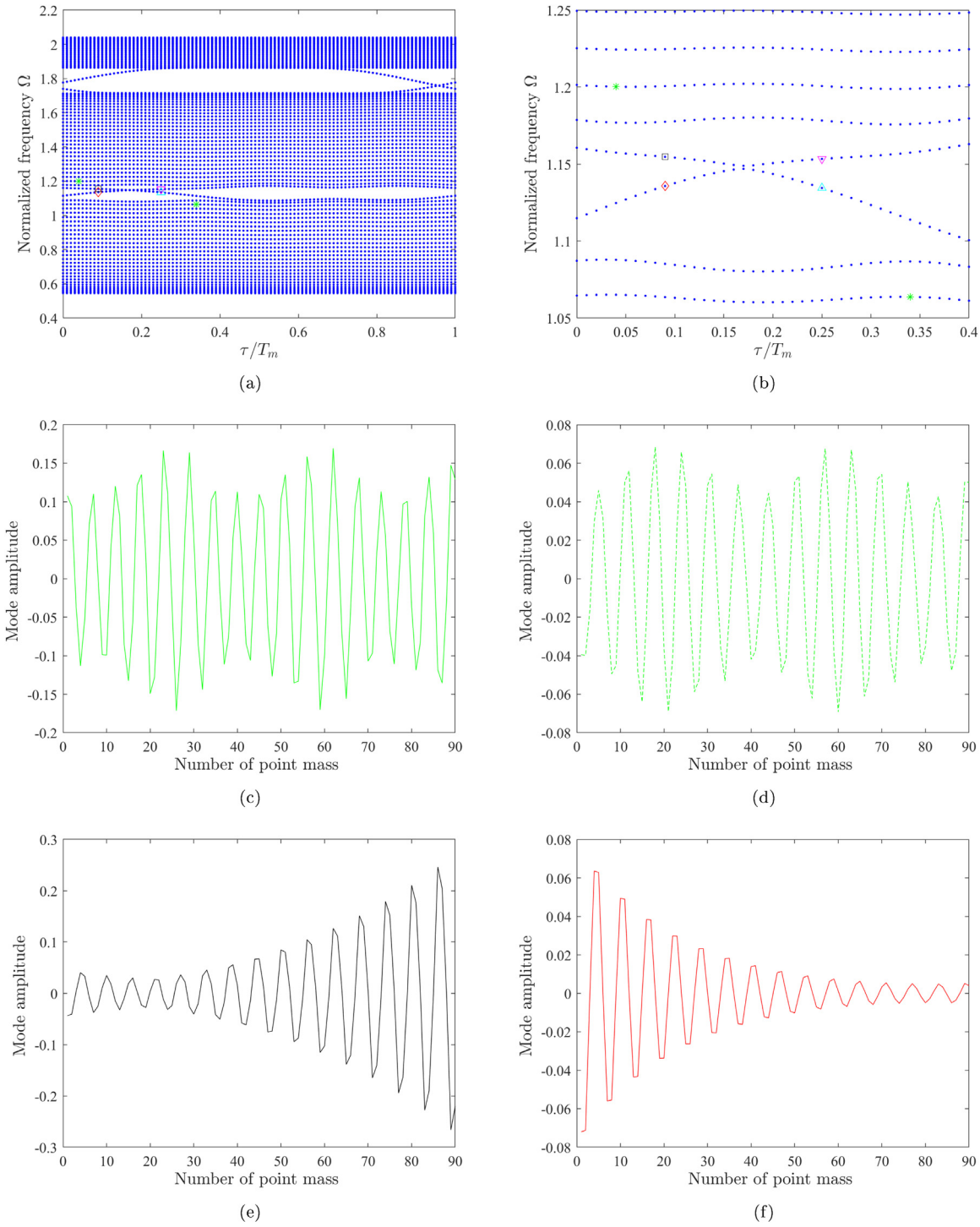

Fig. 10. Evolution of eigenfrequencies and spatial profiles of the corresponding edge modes of a 3-periodic modulated finite periodic lattice (30 UCs) with inerters, over one period of modulation. Two main band gaps (if the zero band gap is neglected) are visible and crossed by the eigenfrequencies of edge states. The regions with dense blue dots denote the bulk pass bands. Panel (b) shows a magnified first band gap in the range of edge mode eigenfrequencies around $0.2T_m$ where green dots highlight the chosen eigenfrequencies of the bulk modes while the black and red squares are eigenfrequencies of the right and left edge modes, respectively. Panels (c)-(f) are the spatial profiles of the corresponding bulk and edge modes. (For interpretation of the references to colour in this figure legend, the reader is referred to the web version of this article.)

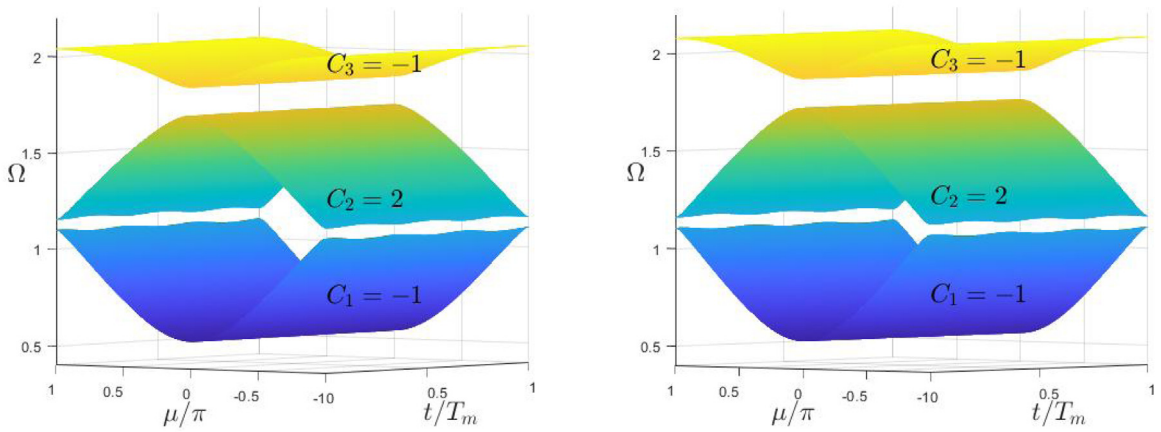

(a) Configuration with inerters (b) Configuration without inerters

Fig. 11. Evolution of dispersion curves of the phononic mass-spring-inerter system with time varying stiffness properties.

not depend on the smoothness of the eigenvectors since only the derivatives of mass and stiffness matrices are involved. Following this line, we used a similar form of the "numerically gauge-invariant" equation for the calculation of Chern numbers which takes the form

$$C_n = \frac{1}{2\pi} \int_{-\pi}^{\pi} \int_{0}^{T} B_n dq dt, \tag{30}$$

where B_n denotes the Berry curvature defined in Appendix 2. It should be noted that the equation for the Berry curvature derived in this paper differs from those shown in [46] since it involves the term with the first derivative of a mass matrix with respect to the wavenumber. The reason for this is that in our case mass matrix is both wavenumber- and time-dependent due to the introduced time-modulated inerter elements.

Figure 11 shows the effect of inerters on the evolution of dispersion curves as a function of the dimensionless wavenumber and time for an inerter-based lattice with 3-periodic modulation of stiffness properties. The following parameters are used in simulations $\beta_m = 0.15$, $\beta_{gm} = 0.5$, $s = 0.01$, $\gamma_g = 0.3$, $\rho_m = 0.01$, as well as the modulation frequency $\Omega_m = 0.2$. The separated dispersion bands can be identified by the Chern numbers based on the Eq. (30) that yield the following integer values $C_1 = -1$, $C_2 = 2$ and $C_3 = -1$ for the first three bands (see Fig. 11). When comparing the evolution of dispersion curves in time for the configuration without and with inerters, one can observe the shifting of branches to lower frequencies in the latter case, which is more pronounced for the higher-frequency branches. This is in line with the result obtained in the previous section. In both configurations, with (Fig. 11a) and without inerters (Fig. 11b), the same Chern numbers are obtained for each band, which implies that by introducing inerters the topological properties of edge states are kept, while at the same time eigenfrequencies of bands are shifted to lower values. However, it should be noted that we were able to retain integer Chern numbers only for the lower values of the inertia amplification parameter (Fig. 11a) which means that the topology is very sensitive to changes in inertia properties of the system. This issue should be investigated further, which would require additional parametric stability analyses that exceed the scope of this study.

6. Conclusion

In this study, we have demonstrated how non-reciprocal wave propagation can occur in different types of time-modulated elastic lattices. We successfully introduced inerter elements in such latices that can be used to shift the dispersion curves frequencies to lower values. Two types of one-dimensional lattices are investigated. The first type includes discrete phononic and locally resonant lattices with mass-inerter-spring elements connected into the mechanical chain while the second type includes discrete-continuous phononic lattice based on the system of parallelly connected Euler-Bernoulli beams coupled through discrete spring-inerter elements. The Bloch-based procedure is suggested to study the dispersion characteristics of observed lattices with simultaneous time-modulation of stiffness and mass properties. Based on this analysis, the existence of asymmetric band gaps is confirmed and used as a basis for transient analysis and demonstration of uni-directional wave propagation.

We additionally computed the topologically invariant Chern numbers of a simple time-modulated discrete phononic lattice based on the derived analytical expression for the Berry curvature that accounts for the time- and wavenumber-dependent properties of the mass matrix. The bulk-edge correspondence principle is used to characterize the one-way topological elastic waves localized at the boundaries of the time-modulated finite lattice. Moreover, we suggested a coupled beam system with inerters that can serve as an ideal platform to implement time-modulated stiffness properties in the classical mechanical context only by applying the periodic axial loads on beams. This fact, along with the introduction of

the inerter elements, can be considered as the main contribution of this work, therefore, showing huge potential for future applications such as tuning of dispersion characteristics of time-modulated elastic lattices.

Data Availability

No data was used for the research described in the article.

Acknowledgments

DK and SP acknowledge the support by the Serbian Ministry of Education, Science and Technological Development through the Mathematical Institute of the Serbian Academy of Sciences and Arts. MC and SA acknowledge funding from European Union's Horizon 2020 research and innovation programme under the Marie Sklodowska-Curie grant agreement No. 896942 (METASINK). JC acknowledges the support from the European Research Council (ERC) through the Starting Grant No. 714577 PHONOMETA and from the MINECO through a Ramón y Cajal grant (Grant No. RYC-2015-17156). JC also acknowledges the support from the Comunidad de Madrid (Spain) - multiannual agreement with UC3M ("Excelencia para el Profesorado Universitario" - EPUC3M14) - Fifth regional research plan 2016–2020.

Appendix A. The components of the interactions matrices

The mass and stiffness matrices for the left and the right interactions are given in the following form

$$\mathbf{M}^{(l)}(t)=\begin{bmatrix}0&0&-sV_3(t)&0&0&0\\0&0&0&0&0&0\\0&0&0&0&0&0\\0&0&0&0&0&0\\0&0&0&0&0&0\\0&0&0&0&0&0\end{bmatrix},\quad \mathbf{M}^{(r)}(t)=\begin{bmatrix}0&0&0&0&0&0\\0&0&0&0&0&0\\-sV_3(t)&0&0&0&0&0\\0&0&0&0&0&0\\0&0&0&0&0&0\\0&0&0&0&0&0\end{bmatrix}, \tag{A.1}$$

$$\mathbf{C}^{(l)}(t)=\begin{bmatrix}0&0&-sE_3(t)&0&0&0\\0&0&0&0&0&0\\0&0&0&0&0&0\\0&0&0&0&0&0\\0&0&0&0&0&0\\0&0&0&0&0&0\end{bmatrix},\quad \mathbf{C}^{(r)}(t)=\begin{bmatrix}0&0&0&0&0&0\\0&0&0&0&0&0\\-sE_3(t)&0&0&0&0&0\\0&0&0&0&0&0\\0&0&0&0&0&0\\0&0&0&0&0&0\end{bmatrix}, \tag{A.2}$$

$$\mathbf{K}^{(l)}(t)=\begin{bmatrix}0&0&-C_3(t)&0&0&0\\0&0&0&0&0&0\\0&0&0&0&0&0\\0&0&0&0&0&0\\0&0&0&0&0&0\\0&0&0&0&0&0\end{bmatrix},\quad \mathbf{K}^{(r)}(t)=\begin{bmatrix}0&0&0&0&0&0\\0&0&0&0&0&0\\-C_3(t)&0&0&0&0&0\\0&0&0&0&0&0\\0&0&0&0&0&0\\0&0&0&0&0&0\end{bmatrix}. \tag{A.3}$$

Appendix B. Berry's curvature

For the determination of the Berry's curvature for the presented time-modulated lattice, the starting point is to define the vector of the Berry connection according to the Nassar et al. [46] in the following form

$$\mathcal{A}_n^{\tau}=\dot{\gamma}_n=Im\langle\Psi_n,\mathbf{M},\dot{\Psi}_n\rangle, \tag{B.1}$$

and

$$\mathcal{A}_n^{\mu}=Im\langle\Psi_n,\mathbf{M},\partial_\mu\Psi_n\rangle, \tag{B.2}$$

Following the methodology given in Nasar et al. [46], the Berry's curvature when the mass matrix is time- and wavenumber-dependent $\mathbf{M}=\mathbf{M}(\tau,\mu)$ is determined as

$$\mathcal{B}_n=2Im\left\{\langle\partial_\mu\Psi_n,\mathbf{M},\dot{\Psi}_n\rangle-\frac{1}{2}\langle\Psi_n,\dot{\mathbf{M}},\partial_\mu\Psi_n\rangle+\frac{1}{2}\langle\Psi_n,\partial_\mu\mathbf{M},\dot{\Psi}_n\rangle\right\}. \tag{B.3}$$

By expanding along the orthogonal eigenstates Ψ_m, the Berry's curvature takes a new form

$$\mathcal{B}_n=\sum_{m\neq n}2Im\{\langle\partial_\mu\Psi_n,\mathbf{M},\Psi_m\rangle\langle\Psi_m,\mathbf{M},\dot{\Psi}_n\rangle-\frac{1}{2}\langle\Psi_n,\dot{\mathbf{M}},\Psi_m\rangle\langle\Psi_m,\mathbf{M},\partial_\mu\Psi_n\rangle \tag{B.4}$$

$$+\frac{1}{2}\langle\Psi_n,\partial_\mu\mathbf{M},\Psi_m\rangle\langle\Psi_m,\mathbf{M},\dot{\Psi}_n\rangle\}.$$

In order to get the Berry's curvature in the most simple form for computational implementation, we are going to remove any derivation of the eigenvectors from the Eq. (B.4), where

$$\langle \Psi_m, \mathbf{M}, \dot{\Psi}_n \rangle = \frac{\langle \Psi_m, \dot{\mathbf{K}}, \Psi_n \rangle - \omega_n^2 \langle \Psi_m, \dot{\mathbf{M}}, \Psi_n \rangle}{\omega_n^2 - \omega_m^2}, \tag{B.5}$$

$$\langle \Psi_m, \mathbf{M}, \partial_\mu \Psi_n \rangle = \frac{\langle \Psi_m, \partial_\mu \mathbf{K}, \Psi_n \rangle - \omega_n^2 \langle \Psi_m, \partial_\mu \mathbf{M}, \Psi_n \rangle}{\omega_n^2 - \omega_m^2}.$$

Appendix C. Finite difference method for time responses

For validation of the specific asymmetric band gap obtained for the time-modulated inerter-based lattice structures, the numerical simulations of the time responses of the inerter-based lattice structures were conducted by using the finite difference method. It showed uni-directional wave propagation for the specific frequency adopted from the asymmetric band gap obtained by the Floquet-Bloch procedures. The time responses are determined for 70 coupled UCs with Born-Karman boundary conditions in order to remove reflections from the edges of lattices. In the case of the lattice based on inerters and beam elements, the total number of the UCs coupled together is 50, with Born-Karman boundary conditions at the end of the lattices.

Introducing the dimensionless time $\tau = \omega_0 t$ and $\omega_m t = \Omega_m \tau$ into the system of differential equations obtained for the whole structure, we can get a new system of equations with harmonic excitation positioned on the half-length of the lattice, that is

$$\mathbf{M}(\tau)\ddot{\mathbf{q}}(\tau) + \mathbf{C}(\tau)\dot{\mathbf{q}}(\tau) + \mathbf{K}(\tau)\mathbf{q}(\tau) = \mathbf{f}(\tau), \tag{C.1}$$

where $\mathbf{M}(\tau)$ is the time dependent mass matrix, $\mathbf{K}(\tau)$ is the stiffness matrix, $\mathbf{C}(\tau)$ time-modulated inerter matrix and $\mathbf{f}(\tau)$ is the vector of external excitation load for a finite dimension lattice. The displacement vector is denoted by $\mathbf{q}$.

By using the finite difference procedure for determination of the time-response of the inerter-based lattices, the second and first derivative of the displacement vector can be approximated in the following manner

$$\ddot{\mathbf{q}}(\tau) = \frac{\mathbf{q}(\tau + h) - 2\mathbf{q}(\tau) + \mathbf{q}(\tau - h)}{h^2}, \tag{C.2}$$

$$\dot{\mathbf{q}}(\tau) = \frac{\mathbf{q}(\tau + h) + \mathbf{q}(\tau - h)}{2h},$$

where h is the time increment.

By introducing the Eq. (B.7) into Eq. (B.6), for zero initial conditions we can get a recursive equation for the displacement vector as

$$\mathbf{q}(\tau + h) = -\mathbf{R}^{-1}(\tau)\mathbf{P}(t)\mathbf{q}(\tau - h) - \mathbf{R}^{-1}(\tau)\mathbf{G}(\tau)\mathbf{q}(\tau) - \mathbf{R}^{-1}(\tau)\mathbf{f}(\tau), \tag{C.3}$$

in which

$$\mathbf{R}(\tau) = \frac{1}{h^2}\mathbf{M}(\tau) + \frac{1}{2h}\mathbf{C}(\tau), \quad \mathbf{P}(\tau) = \frac{1}{h^2}\mathbf{M}(\tau) - \frac{1}{2h}\mathbf{C}(\tau), \quad \mathbf{G}(\tau) = \mathbf{K}(\tau) - \frac{2}{h^2}\mathbf{M}(\tau).$$

For all the simulation we adopt the following initial conditions $\mathbf{q}(0) = \mathbf{0}$ and $\dot{\mathbf{q}}(0) = \mathbf{0}$.

References

[1] C. Lim, et al., From photonic crystals to seismic metamaterials: a review via phononic crystals and acoustic metamaterials, Arch. Comput. Methods Eng. (2021) 1–62.
[2] H.M. Kolken, S. Janbaz, S.M. Leeflang, K. Lietaert, H.H. Weinans, A.A. Zadpoor, Rationally designed meta-implants: a combination of auxetic and conventional meta-biomaterials, Mater. Horiz. 5 (1) (2018) 28–35.
[3] Z. Chen, B. Guo, Y. Yang, C. Cheng, Metamaterials-based enhanced energy harvesting: areview, Physica B 438 (2014) 1–8.
[4] M.I. Hussein, M.J. Leamy, M. Ruzzene, Dynamics of phononic materials and structures: historical origins, recent progress, and future outlook, Appl. Mech. Rev. 66 (4) (2014).
[5] Y.-F. Wang, Y.-Z. Wang, B. Wu, W. Chen, Y.-S. Wang, Tunable and active phononic crystals and metamaterials, Appl. Mech. Rev. 72 (4) (2020) 040801.
[6] M.I. Rosa, R.K. Pal, J.R. Arruda, M. Ruzzene, Edge states and topological pumping in spatially modulated elastic lattices, Phys. Rev. Lett. 123 (3) (2019) 034301.
[7] X. Ni, K. Chen, M. Weiner, D.J. Apigo, C. Prodan, A. Alu, E. Prodan, A.B. Khanikaev, Observation of hofstadter butterfly and topological edge states in reconfigurable quasi-periodic acoustic crystals, Commun. Phys. 2 (1) (2019) 1–7.
[8] H. Nassar, B. Yousefzadeh, R. Fleury, M. Ruzzene, A. Alù, C. Daraio, A.N. Norris, G. Huang, M.R. Haberman, Nonreciprocity in acoustic and elastic materials, Nat. Rev. Mater. 5 (9) (2020) 667–685.
[9] S. Taravati, A.A. Kishk, Space-time modulation: principles and applications, IEEE Microw. Mag. 21 (4) (2020) 30–56.
[10] M. Attarzadeh, M. Nouh, Non-reciprocal elastic wave propagation in 2D phononic membranes with spatiotemporally varying material properties, J. Sound Vib. 422 (2018) 264–277.
[11] F. Hakim, M. Ramezani, S. Rassay, R. Tabrizian, A non-reciprocal lamb-wave delay line exploiting acoustoelectric effect in single crystal germanium, in: 2020 IEEE 33rd International Conference on Micro Electro Mechanical Systems (MEMS), IEEE, 2020, pp. 1246–1249.
[12] M. Ansari, M. Attarzadeh, M. Nouh, M.A. Karami, Application of magnetoelastic materials in spatiotemporally modulated phononic crystals for nonreciprocal wave propagation, Smart Mater. Struct. 27 (1) (2017) 015030.

[13] J. Li, C. Shen, X. Zhu, Y. Xie, S.A. Cummer, Nonreciprocal sound propagation in space-time modulated media, Phys. Rev. B 99 (14) (2019) 144311.
[14] J.A. Richards, Analysis of Periodically Time-Varying Systems, Springer Science & Business Media, 2012.
[15] J. Vila, R.K. Pal, M. Ruzzene, G. Trainiti, A Bloch-based procedure for dispersion analysis of lattices with periodic time-varying properties, J. Sound Vib. 406 (2017) 363–377.
[16] J. Huang, X. Zhou, A time-varying mass metamaterial for non-reciprocal wave propagation, Int. J. Solids Struct. 164 (2019) 25–36.
[17] J. Huang, X. Zhou, Non-reciprocal metamaterials with simultaneously time-varying stiffness and mass, J. Appl. Mech. 87 (7) (2020) 071003.
[18] H. Nassar, H. Chen, A. Norris, M. Haberman, G. Huang, Non-reciprocal wave propagation in modulated elastic metamaterials, Proc. R. Soc. A Math.Phys. Eng. Sci. 473 (2202) (2017) 20170188.
[19] G. Trainiti, M. Ruzzene, Non-reciprocal elastic wave propagation in spatiotemporal periodic structures, New J. Phys. 18 (8) (2016) 083047.
[20] E. Riva, M. Di Ronco, A. Elabd, G. Cazzulani, F. Braghin, Non-reciprocal wave propagation in discretely modulated spatiotemporal plates, J. Sound Vib. 471 (2020) 115186.
[21] E. Riva, J. Marconi, G. Cazzulani, F. Braghin, Generalized plane wave expansion method for non-reciprocal discretely modulated waveguides, J. Sound Vib. 449 (2019) 172–181.
[22] M. Attarzadeh, M. Nouh, Elastic wave propagation in moving phononic crystals and correlations with stationary spatiotemporally modulated systems, AIP Adv. 8 (10) (2018) 105302.
[23] Y.-T. Wang, Y.-W. Tsai, W. Gao, Floquet topological photonic crystals with temporally modulated media, Opt. Express 28 (14) (2020) 21268–21274.
[24] S. Taravati, N. Chamanara, C. Caloz, Nonreciprocal electromagnetic scattering from a periodically space-time modulated slab and application to a quasisonic isolator, Phys. Rev. B 96 (16) (2017) 165144.
[25] G. Trainiti, Y. Xia, J. Marconi, G. Cazzulani, A. Erturk, M. Ruzzene, Time-periodic stiffness modulation in elastic metamaterials for selective wave filtering: theory and experiment, Phys. Rev. Lett. 122 (12) (2019) 124301.
[26] Y. Chen, X. Li, H. Nassar, A.N. Norris, C. Daraio, G. Huang, Nonreciprocal wave propagation in a continuum-based metamaterial with space-time modulated resonators, Phys. Rev. Appl. 11 (6) (2019) 064052.
[27] M. Attarzadeh, J. Callanan, M. Nouh, Experimental observation of nonreciprocal waves in a resonant metamaterial beam, Phys. Rev. Appl. 13 (2) (2020) 021001.
[28] M. Attarzadeh, H. Al Ba'ba'a, M. Nouh, On the wave dispersion and non-reciprocal power flow in space-time traveling acoustic metamaterials, Appl. Acoust. 133 (2018) 210–214.
[29] K.A. Lurie, An Introduction to the Mathematical Theory of Dynamic Materials, 2nd ed., Springer, 2017.
[30] F. Sun, L. Xiao, Bandgap characteristics and seismic applications of inerter-in-lattice metamaterials, J. Eng. Mech. 145 (9) (2019) 04019067.
[31] H. Al Ba'ba'a, D. DePauw, T. Singh, M. Nouh, Dispersion transitions and pole-zero characteristics of finite inertially amplified acoustic metamaterials, J. Appl. Phys. 123 (10) (2018) 105106.
[32] M.C. Smith, Synthesis of mechanical networks: the inerter, IEEE Trans. Automat. Control 47 (10) (2002) 1648–1662.
[33] M.C. Smith, The inerter: a retrospective, Annu. Rev. Control Rob. Auton.Syst. 3 (2020) 361–391.
[34] C. Papageorgiou, N.E. Houghton, M.C. Smith, Experimental testing and analysis of inerter devices, J. Dyn. Syst. Meas. Control 131 (1) (2009).
[35] E.D. John, D.J. Wagg, Design and testing of a frictionless mechanical inerter device using living-hinges, J. Franklin Inst. 356 (14) (2019) 7650–7668.
[36] D.J. Wagg, A review of the mechanical inerter: historical context, physical realisations and nonlinear applications, Nonlinear Dyn. (2021) 1–22.
[37] P.P. Kulkarni, J.M. Manimala, Longitudinal elastic wave propagation characteristics of inertant acoustic metamaterials, J. Appl. Phys. 119 (24) (2016) 245101.
[38] D. Mu, H. Shu, L. Zhao, S. An, A review of research on seismic metamaterials, Adv. Eng. Mater. 22 (4) (2020) 1901148.
[39] X. Fang, K.-C. Chuang, X. Jin, Z. Huang, Band-gap properties of elastic metamaterials with inerter-based dynamic vibration absorbers, J. Appl. Mech. 85 (7) (2018) 071010.
[40] A. Banerjee, S. Adhikari, M.I. Hussein, Inertial amplification band-gap generation by coupling a levered mass with a locally resonant mass, Int. J. Mech. Sci. 207 (2021) 106630.
[41] V.R. Challa, M. Prasad, Y. Shi, F.T. Fisher, A vibration energy harvesting device with bidirectional resonance frequency tunability, Smart Mater. Struct. 17 (1) (2008) 015035.
[42] M.I. Hussein, I. Patrick, A. Banerjee, S. Adhikari, Metadamping in inertially amplified metamaterials: trade-off between spatial attenuation and temporal attenuation, J. Sound Vib. 531 (2022) 116977.
[43] P. Hagedorn, A. DasGupta, Vibrations and Waves in Continuous Mechanical Systems, Wiley Online Library, 2007.
[44] G.-C. Zhang, H. Ding, L.-Q. Chen, S.-P. Yang, Galerkin method for steady-state response of nonlinear forced vibration of axially moving beams at supercritical speeds, J. Sound Vib. 331 (7) (2012) 1612–1623.
[45] D. Karličić, M. Cajić, S. Paunović, S. Adhikari, Bloch waves in an array of elastically connected periodic slender structures, Mech. Syst. Signal Process. 155 (2021) 107591.
[46] H. Nassar, H. Chen, A. Norris, G. Huang, Quantization of band tilting in modulated phononic crystals, Phys. Rev. B 97 (1) (2018) 014305.